JCI insight

Pregnancy dedifferentiates memory CD8$^+$ T cells into hypofunctional cells with exhaustion-enriched programs

Jared M. Pollard, … , Maria-Luisa Alegre, Anita S. Chong

JCI Insight. 2024. https://doi.org/10.1172/jci.insight.176381.

Research In-Press Preview **Immunology** **Transplantation**

Alloreactive memory, unlike naïve, CD8$^+$ T cells resist transplantation tolerance protocols and are a critical barrier to long-term graft acceptance in the clinic. We here show that semi-allogeneic pregnancy successfully reprogrammed memory fetus/graft-specific CD8$^+$ T cells (T_{FGS}) towards hypofunction. Female C57BL/6 mice harboring memory CD8$^+$ T cells generated by the rejection of BALB/c skin grafts and then mated with BALB/c males achieved rates of pregnancy comparable to naive controls. Post-partum fetus/graft-specific CD8$^+$ T cells (T_{FGS}) from skin-sensitized dams upregulated expression of T cell exhaustion (T_{EX}) markers (Tox, Eomes, PD-1, TIGIT, and Lag3). Transcriptional analysis corroborated an enrichment of canonical T exhaustion (T_{EX}) genes in post-partum memory T_{FGS} and additionally, revealed a downregulation of a subset of memory-associated transcripts. Strikingly, pregnancy induced extensive epigenetic modifications of exhaustion- and memory-associated genes in memory T_{FGS}, whereas minimal epigenetic modifications were observed in naive T_{FGS} cells. Finally, post-partum memory T_{FGS} durably expressed the exhaustion-enriched phenotype, and their susceptibility to transplantation tolerance was significantly restored compared to memory T_{FGS}. These findings advance the concept of pregnancy as an epigenetic modulator inducing hypofunction in memory CD8$^+$ T cells that has relevance not only for pregnancy and transplantation tolerance, but also for tumor immunity and chronic infections.

Pregnancy dedifferentiates memory CD8$^+$ T cells into hypofunctional cells with exhaustion-enriched programs

Jared M. Pollard[1], Grace Hynes[1], Dengping Yin[1], Malay Mandal[2], Fotini Gounari[2,3], Maria-Luisa Alegre[2], Anita Chong[1]

[1]Section of Transplantation, Department of Surgery, University of Chicago, Chicago IL, USA

[2]Section of Rheumatology, Department of Medicine, University of Chicago, Chicago IL, USA

[3]Department of Immunology, Mayo Clinic, Phoenix AZ, USA

Authorship note: JMP an GH are co-first authors. MLA and AC are co-senior authors.

Abstract

Alloreactive memory, unlike naïve, $CD8^+$ T cells resist transplantation tolerance protocols and are a critical barrier to long-term graft acceptance in the clinic. We here show that semi-allogeneic pregnancy successfully reprogrammed memory fetus/graft-specific $CD8^+$ T cells (T_{FGS}) towards hypofunction. Female C57BL/6 mice harboring memory $CD8^+$ T cells generated by the rejection of BALB/c skin grafts and then mated with BALB/c males achieved rates of pregnancy comparable to naive controls. Post-partum fetus/graft-specific $CD8^+$ T cells (T_{FGS}) from skin-sensitized dams upregulated expression of T cell exhaustion (T_{EX}) markers (Tox, Eomes, PD-1, TIGIT, and Lag3). Transcriptional analysis corroborated an enrichment of canonical T exhaustion (T_{EX}) genes in post-partum memory T_{FGS} and additionally, revealed a downregulation of a subset of memory-associated transcripts. Strikingly, pregnancy induced extensive epigenetic modifications of exhaustion- and memory-associated genes in memory $T_{FGS,}$ whereas minimal epigenetic modifications were observed in naive T_{FGS} cells. Finally, post-partum memory T_{FGS} durably expressed the exhaustion-enriched phenotype, and their susceptibility to transplantation tolerance was significantly restored compared to memory T_{FGS}. These findings advance the concept of pregnancy as an epigenetic modulator inducing hypofunction in memory $CD8^+$ T cells that has relevance not only for pregnancy and transplantation tolerance, but also for tumor immunity and chronic infections.

Introduction

Mammalian pregnancy has long been recognized as a model of spontaneous alloantigen-specific tolerance, whereby the maternal adaptive immune system must rapidly regulate responses towards the semi-allogeneic fetus to preserve fetal viability (1, 2). Maternal T cell tolerance is characterized by the upregulation of coinhibitory markers and inhibition of pro-inflammatory cytokine production in $CD4^+FoxP3^-$ conventional T cells (T_{convs}), as well as the expansion of fetus-specific $CD4^+FoxP3^+$ regulatory T cells (T_{regs}) that are protective in primary and secondary pregnancies (3-5). Notably, while pregnancy efficiently tolerizes naive fetus-specific T cells, it simultaneously induces humoral sensitization. We showed that pregnancy-induced a state of T cell tolerance that was sufficient to mediate the spontaneous acceptance of subsequently transplanted offspring-matched heart grafts, but only if B cells and fetus-specific antibodies are absent (3). Subsequently, Lewis et al. reported that naive OVA-reactive TCR-transgenic OT-I $CD8^+$ T cells acquired an exhausted transcriptional signature after pregnancy with OVA-expressing progeny (6), while Kinder et al. showed that endogenous OVA-reactive $CD8^+$ T cell expression of PD-1 and Lag-3 acquired during primary pregnancy protected against fetal wastage in a secondary pregnancy (7).

In contrast to pregnancy, semi-allogeneic organ transplants stimulate alloreactive $CD4^+$ and $CD8^+$ T cells that mediate graft rejection, with $CD4^+$ T cells promoting B cell and $CD8^+$ T cell responses as well as secreting pro-inflammatory cytokines and chemokines, and $CD8^+$ T cells play pro-inflammatory and cytotoxic roles (8-11). Alloreactive memory T cells are generated by exposure to allogeneic MHC following transplantation or blood transfusion, or through heterologous immunity, wherein T cells primed by infections or environmental antigens cross-react with donor MHC (12-15). As a result, most humans harbor memory alloreactive T cells, and their frequency increases with age (8). Importantly, memory T cells antagonize therapies that successfully induce transplantation tolerance in naive mice by resisting the induction of cell-intrinsic hypofunction achieved in naive T cells (16-18). Indeed, we recently reported that the presence of memory T cells sensitized to a single donor antigen mediated linked sensitization and were sufficient to prevent co-stimulation blockade-induced transplantation tolerance to a multiple mismatch

allograft (19). Thus, the potent barrier posed by alloreactive memory T cells to transplantation tolerance underscores the critical need to identify mechanisms for tolerizing memory T cell responses (20-23) .

The critical role of memory $CD8^+$ T cells in mediating allograft rejection, inducing spontaneous abortions, and antagonizing tolerance, prompted this proof-of-principle study to test whether pregnancy can successfully program hypofunction into memory fetus/graft-specific $CD8^+$ T cells (T_{FGS}) (8-11, 24, 25). We show that despite the presence of rejection-induced memory $CD4^+$, $CD8^+$ and B cell responses, sensitized female mice consistently achieved spontaneous tolerance towards the semi-allogeneic fetus, achieving pregnancy success rates comparable to those of naive mice. We then used high-dimensional multi-omics approaches to show that pregnancy dedifferentiates memory $CD8^+$ T cells into hypofunctional cells with an exhaustion phenotype and reduced expression of a subset of memory genes. The pregnancy-programmed hypofunctional phenotype in memory T_{FGS} was resistant to NFAT inhibition, associated with extensive epigenetic remodeling, persisted post-partum, and manifested as restored susceptibility to co-stimulation blockade-mediated transplantation tolerance. Taken together, our findings highlight the evolutionary robustness of mammalian pregnancy in constraining fully established allogeneic memory responses and introduces a potentially novel hypothesis that successful reprogramming of memory $CD8^+$ T cells towards hypofunction requires the epigenetic imprinting of exhaustion circuits and reduced expression of a subset of memory genes. The conceptual foundation provided here brings us closer to understanding and therapeutically harnessing mechanisms of antigen-specific T cell hypofunction to substantially reduce the barrier that memory $CD8^+$ T cells pose to transplantation tolerance.

Results

Pregnancy successfully constrains immunological memory

To test whether semi-allogeneic pregnancy is possible in females harboring immunological memory to paternal antigens, we sensitized female C57Bl/6 (B6, H-2^b) mice with skins transplants (skinTx) from fully-mismatched male BALB/c mice. Female B6 mice rejected BALB/c skin grafts within 10 days (data not shown), and at day ≥30 post-transplantation, they were mated with BALB/c males (rejection+pregnancy; R+P). The rates of successful pregnancy, including multiple successive pregnancies, were comparable between R+P and control naive mice mated with BALB/c males (pregnancy only; P) and no differences in resulting viable pups were observed (Figure 1a,b). Thus, pregnancy is able to constrain memory immune responses elicited by the rejection of fully-mismatched skin allografts to permit successful tolerance of the semi-allogeneic fetus.

Pregnancy induces the expression of co-inhibitory molecules in memory T_{FGS}

To gain insights into pregnancy-imposed hypofunction we tracked a tracer population of endogenous, polyclonal fetus-reactive $CD8^+$ T cells that recognize the model 2W-OVA antigen expressed by the sensitizing skin and fetus. We sensitized B6 females with 2W-OVA.BALB/c (H-2^d) skins and then mated them with 2W-OVA.BALB/c (H-2^d) males (Fig 1c). OVA-specific $CD8^+$ T cells were identified by flow cytometry using double fluorophore-labeled OVA:K^b tetramers; henceforth, these fetus- and graft-specific T cells are referred to as T_{FGS} (26, 27). We note that OVA expressed by the skin or F1 fetus is cross-presented by recipient/dam APCs, although it is possible that maternal APCs are cross-decorated with OVA:K^b complexes from F1 cells, or that microchimeric fetal cells are presenting OVA:K^b to maternal T cells (7, 28).

We designed a 19-color spectral flow cytometry panel to probe the expression of activation, memory, co-inhibitory and anergy markers by fetus (OVA)-specific T_{FGS} from naive (N), P, skin rejection (R) and R+P groups (Supplementary Table 1). OVA-specific $CD8^+$ T cells were analyzed on day 30+ post-skinTx for R mice, or at post-partum day 0-3 for P and R+P mice. We observed a significant increase in

T_{FGS} recovery from R+P mice compared to P mice (Figure 1d, e). Despite this expansion, R+P T_{FGS} displayed elevated expression of multiple coinhibitory markers compared to R T_{FGS}, including PD-1, LAG3, TIGIT, and FR4 (Figure 1f, Extended Data Figure 1a-b). In contrast, P T_{FGS} preferentially upregulated both anergy markers, CD73 and FR4, as well as LAG3 and PD-1, compared to N T_{FGS}. Finally, only post-partum $CD8^+$ T_{FGS} exhibited this phenotype in response to pregnancy, as the non-OVA-specific $CD8^+$ T cells from P, R and R+P all resembled naïve T cells, thus confirming that the pregnancy-induced phenotype in T_{FGS} is driven by antigen recognition (Figure 1g).

To visualize T_{FGS} phenotypes at single-cell resolution, we used uniform manifold approximation and projection (UMAP) dimensionality reduction and FlowSOM clustering to identify 4 major and 3 minor cell subsets (Figure 1h). As anticipated, N and R T_{FGS} were largely homogenous, with >75% of these cells mapping to Cluster 1 or Cluster 4, respectively (Figure 1i). In contrast, the effect of pregnancy on T_{FGS} was heterogeneous, with ~50% of P and ~25% of R+P T_{FGS} remaining phenotypically similar to N or R T_{FGS}, respectively. Notably, Cluster 5 was identified as a shared cluster induced by pregnancy, comprising ~25% of both P and R+P T_{FGS} and defined by elevated expression of multiple coinhibitory markers, and reduced expression of the proliferation marker Ki67 (Figure 1j, Extended Data Figure 1c). Cluster 7 was unique to R+P T_{FGS} and was similar to Cluster 5 except for reduced CD73 expression. Collectively, these observations support a hypothesis that encounter of alloantigen during pregnancy programs hypofunction in memory T_{FGS} through the induction of higher levels of co-inhibitory exhaustion markers and lower levels of anergy markers compared to post-partum naive T_{FGS}.

Pregnancy induces both distinct and shared transcriptional modifications in naive and memory T_{FGS}

We next tested the hypothesis that the difference in phenotypic markers induced by pregnancy was indicative of a broader set of transcriptional modifications induced in memory vs. naive T_{FGS}. We performed genome-wide transcriptional profiling of flow-sorted T_{FGS} subsets to account for the heterogeneity among pregnancy-modified T_{FGS} while retaining the advantageous sequencing depth of bulk RNA-sequencing.

We sorted OVA-specific T_{FGS} into the 4 predominant phenotypic subsets as illustrated in Fig 1g-h: Cluster 1 (C1, naive-like phenotype), Cluster 4 (C4, rejection-like phenotype), Cluster 5 (C5, shared by P and R+P), and Cluster 7 (C7, unique to R+P) (Figure 2a). The proportions of each cluster in this panel were consistent with our original phenotypic data (Figure 2b-c).

We constructed a heatmap to visualize the transcriptional expression of the markers used in our flow cytometry panel in Figure 1 and observed that the expression patterns in our transcriptional dataset were consistent with phenotypic data (Figure 2d-e). Pregnancy induced comparable levels of *Pdcd1*, and higher levels of exhaustion-associated transcripts *Lag3* and *Tigit* in R+P C5 and C7 compared to P C5. In contrast, P C5 expressed higher levels of the anergy-associated transcripts, Nt5e (CD73) and Izumo1r (FR4) compared to R+P C7.

We next performed differential expression analysis to visualize the global transcriptional differences via UMAP (Figure 2f). R and N T_{FGS} displayed distinct transcriptional signatures, with the P C1 subset nearly identical to N T_{FGS}, and the R+P C4 subset similar to R T_{FGS}. These data corroborate the phenotyping data (Fig 1h-j) that a subset of T_{FGS} remained unmodified by pregnancy in both P and R+P mice. Differentially expressed genes (DEGs) by Cluster C5 T_{FGS} from P and R+P indicated that they were transcriptionally similar, while R+P C7 vs. R+P C5 T_{FGS} were more similar than initially anticipated based on the phenotypic data, sharing ~60% of their transcriptome respectively (Figure 2g).

To reduce complexity, we henceforward focused our subsequent transcriptional analysis on the post-pregnancy cell clusters P C5 and R+P C5, referring to them P and R+P, respectively (Figure 3a). UMAP confirmed that the transcriptomes of these post-partum P and R+P cells were more similar to each other than before pregnancy (Figure 3b). Visualizing the top DEGs between the 4 experimental groups (Naive, P, R, R+P) by heatmap and K-means clustering identified 4 main DEG clusters (Figure 3c, d). Clusters A and C DEG were upregulated by pregnancy in P and R+P compared to N and R T_{FGS} included T_{EX} genes, *Tox, Eomes, Slamf6, Nfatc1/3, Lag3* and *Havcr2* (Tim-3). Cluster B DEGs were downregulated in R and P, and even more so in R+P included *Tcf7* and *Lef1* transcriptional factors that are reduced in exhausted $CD8^+$ T cells (29-31). Interestingly, DEG Cluster D (n=362) was strongly upregulated in R vs. N

but downregulated in R+P T_{FGS} to levels that approached P T_{FGS}. Metascape analysis categorized these DEGs as enriched for negative regulation of inflammatory responses, NK cytotoxicity, regulation of lymphocyte immunity and viral protein interaction genes (Extended Data Figure 2a-e). These DEGs included critical T cell effector genes (*Gzma*, *Prf1*) as well as chemokine genes that control effector T cell migration to tissue sites (*Cxcr3, Ccr5, Ccr6, Ccr2*) (32-35). These data raise the possibility that a subset of memory-associated upregulated transcripts is significantly downregulated by pregnancy.

We next focused our analysis on the unique 817 and 831 DEGs induced by pregnancy, with a 24% transcriptional overlap (n=196), in R+P and P T_{FGS}, respectively (Figure 3e). Visualizing DEGs unique to post-partum memory T_{FGS} via heatmap and volcano plots showed comparable numbers upregulated genes (including exhaustion-associated genes: *Ikzf2* (HELIOS)*, Havcr2* (TIM-3)*,* and downregulated genes (including memory-associated genes: *Lef1, Il7r* (CD127)*,* and *Tcf7l2* (TCF-4)) (Figure 3f; Extended Data Figure 3a) (29-31, 36, 37). Metascape pathway analysis of R+P-unique DEGs (vs. R) indicated an upregulation of the regulatory pathways for cytokine production and T cell differentiation, as well as downregulation of JAK-STAT and Delta-Notch signaling (Extended Data Figure 3b). In contrast, the majority of DEGs unique to P T_{FGS} were upregulated, including *Nfatc3, Ikzf3,* and *Runx2,* and within the T cell co-stimulation and cellular response to IL-18 Metascape pathways (Figure 3f; Extended Data Figure 3c).

Finally, we examined the set of 196 shared DEGs induced by pregnancy in both memory and naive T_{FGS}, with the majority of these shared DEGs being upregulated (168 genes) (Figure 3f). Metascape pathway analysis revealed an enrichment in regulation of cytokine production, and of T cell activation and differentiation (Extended Data Figure 3d). Notable examples included upregulated *Tox, Nfatc1, Il10, Il21* and *Tnfsf4,* and downregulated *Ccr7* and *Satb1* (Extended Data Figure 3e). In contrast, R T_{FGS} displayed distinct transcriptional signatures, with many of the upregulated genes classified in T cell activation and effector function pathways (Extended Data Figure 4a-b). Taken together, these data show that the induction of T cell hypofunction by pregnancy results in shared and distinct transcriptional changes in memory vs. naive T_{FGS}.

Pregnancy elicits an exhausted transcriptional signature in memory T_{FGS}

Lewis et al. (6) recently reported that pregnancy-induced hypofunction in naive OT-I cells was associated with a transcriptional state of exhaustion, prompting us to test whether memory T_{FGS} could be similarly reprogrammed into exhaustion. To this end, we ranked the DEGs induced by pregnancy in memory or naive T_{FGS}, comparing them to hallmark gene sets of exhausted $CD8^+$ T cells (T_{EX}) during chronic infection by Gene Set Enrichment Analysis (GSEA) (Figure 4a) (38). Indeed, we observed a significant enrichment in both upregulated and downregulated T_{EX} signatures in R+P T_{FGS}. Notably, *Tox* and *Tigit* were identified as part of the leading edge of upregulated genes, while *Satb1* and *IL-7r were* in the leading edge of downregulated genes. In contrast, GSEA of the DEGs induced in P T_{FGS} revealed a significant enrichment of only the upregulated T_{EX} signature. As a control, we also ran GSEA on the DEGs of rejection (R vs. N T_{FGS}) and showed that there was no enrichment for any exhaustion gene sets (Extended Data Figure 4c). Taken together, these GSEA analyses supported a more enriched transcriptional response towards exhaustion in post-partum memory compared to naive T_{FGS}, consistent with the hypothesis that more co-inhibition is required to constrain memory T_{FGS}.

We performed GSEA analyses on the distinct and shared DEGs induced by pregnancy in naive and memory T_{FGS}, and compared them with multiple additional T_{EX} gene sets from cancer, chronic infection, and pregnancy (Figure 4c-d, Extended Data Figure 5) (38-40). We corroborated the observation that pregnancy-induced DEGs unique to R+P were enriched for both up- and down-regulated T_{EX} genes, whereas only upregulated T_{EX} transcripts were enriched in P. Furthermore, even within the 196 pregnancy-induced gene set shared by naive and memory T_{FGS}, we observed a statistically significant trend that the relative magnitude of transcriptional change was greater in R+P vs. P T_{FGS} (Figure 4d). Notable examples of DEGs following this trend included Tox, *Tigit, Il10,* IL-21, and *Satb1*. In contrast, only a small subset of genes was more upregulated in P, including *Pdcd1* (PD-1) and *Tnfsf4* (OX40L).

Taken together, our RNA-seq data confirm that pregnancy induces clearly distinct global transcription signatures in memory vs. naive T_{FGS}, with a significantly higher level and more extensive expression of exhaustion-associated transcripts in memory T_{FGS}.

Pregnancy induces distinct phenotypes of hypofunction in memory vs. naive T_{FGS}

We validated our transcriptional findings by developing a larger 23-color spectral flow cytometry panel to assess the phenotypic expression of additional markers identified in our transcriptional analysis (Supplementary Table 1). This panel more readily captured differences between P and R+P T_{FGS}, as illustrated by radar plot and UMAP+FlowSOM (Figure 5a-c), that were not observed in the non-OVA-specific $CD8^+$ T cells (Extended Data Figure 6a). P T_{FGS} (Cluster E) preferentially upregulated the anergy markers, FR4 and CD73, and more modestly upregulated T_{EX} markers, Tox and Eomes, compared to R+P T_{FGS} (Figure 5b-d, Extended Data Figure 6b-g). The majority of R+P T_{FGS} mapped to Clusters C and D, which were characterized by a significantly more robust expression of Tox and Eomes compared to P T_{FGS}. These data highlight the distinct gradation of phenotypic exhaustion markers induced by pregnancy in memory vs. naive $CD8^+$ T_{FGS}.

Observations by Lewis et al. (6) and our observation of induced expression of NFAT in memory vs. naive T_{FGS} prompted us to test whether the phenotypic profiles of exhaustion was dependent on NFAT signaling. We show that treatment with FK506, a pharmacological inhibitor of NFAT, during pregnancy significantly reduced the expression of exhaustion markers, PD-1, Tox, NFATc1, Tigit, SLAMF6, and the anergy marker CD73, in P T_{FGS} consistent with Lewis et al. (6) (Figure 5e, Extended Data Figure 7a-c). Notably, these markers were not significantly inhibited in R+P T_{FGS}, suggesting that the expression of exhaustion/anergy markers in P T_{FGS} is partially dependent on NFAT signaling whereas their expression by R+P T_{FGS} is NFAT-independent. This underscores another difference in how pregnancy affects naive vs. memory T_{FGS} and raises the possibility of differential epigenetic modification driving the T_{EX} phenotype in R+P T_{FGS}.

Pregnancy programs extensive exhaustion-associated chromatin remodeling in memory T_{FGS}, but not in naive T_{FGS}

Because $CD8^+$ T cells undergo epigenetic modifications during the differentiation into effector/memory and exhausted/hypofunctional T cells (37, 41-45), we hypothesized that pregnancy would epigenetically program memory and naive T_{FGS} to sustain their states of hypofunction. We used the same sorting strategy described for RNA-Seq as defined in Figure 2 on fetus/graft-specific T cells to perform the Assay for Transposase-Accessible Chromatin with high-throughput sequencing (ATAC-Seq). Chromatin accessibility heatmaps provided a visualization of global differences between T_{FGS} subsets, while pie charts show comparable genomic distribution of the reproducible ATAC-Seq peaks identified for each T_{FGS} cluster (Extended Data Figure 8a-b). An Upset plot showed the total number of reproducible peaks shared by various combinations of T_{FGS} subsets, noting unique peaks present only in R+P C5 and/or C7 T_{FGS} (Extended Data Figure 8c).

By visualizing the Differentially Accessible Peaks (DAPs) using UMAP and heatmap with K-means clustering, we show that N vs. R T_{FGS} had distinct chromatin accessibility profiles (K-means clusters A-B) consistent with the acquisition of a memory T cell epigenome (Extended Data Figure 9a-d). These clusters grouped loci that were remodeled in R and more extensively in post-partum memory (R+P) T_{FGS}. In contrast, K-means cluster C grouped loci that were closed in N, P, R, and the R+P C4 ($PD\text{-}1^{neg}$) subsets, but significantly opened in R+P C5 and C7 T_{FGS}. Finally, K-means cluster D loci were open in N, P, and R subsets but closed in R+P T_{FGS} (46-49). Collectively, these observations support the hypothesis that pregnancy imposed more extensive epigenetic modulation in memory vs. naive T_{FGS}.

To more rigorously address the hypothesis that epigenetic modifications in R+P but not P T_{FGS} occurred during pregnancy, we leveraged our RNA-Seq dataset from Fig 3c to assess chromatin remodeling associated with pregnancy-induced DEGs in P or R+P T_{FGS}. At the loci of all DEGs (n=831) uniquely induced in naive T_{FGS} by pregnancy, we observed no significant change in chromatin accessibility

(Fig 6a). In contrast, significant increases and decreases in chromatin accessibility in the DEGs (n=817) induced by pregnancy in memory T_{FGS}, corresponding to transcriptional up- and down-regulation, respectively (Figure 6b). These observations support the hypothesis that exhaustion transcriptome was associated with extensive pregnancy-mediated chromatin remodeling uniquely in memory T_{FGS}, while the exhaustion transcriptome in naive T_{FGS} required minimal chromatin remodeling.

Supporting this conclusion, chromatin accessibility of the 196 shared DEGs induced by pregnancy and enriched for T_{EX} in R+P and P T_{FGS} was also significantly changed in R+P vs. R T_{FGS}, but not in P vs. N T_{FGS} (Figure 6c, d). Notably, pregnancy-mediated chromatin remodeling remained detectable at distances of up to 100kb from the transcription start sites of these loci, supporting the possibility of both proximal remodeling of the locus itself and distal enhancer remodeling (Figure 6e). These differences are readily apparent when visualizing individual exhaustion-associated loci such as *Tox* and *Maf,* where multiple open peaks were present in R+P T_{FGS} but not in R or P T_{FGS} (Figure 6f-g) (36, 37, 40, 50, 51). Chromatin accessibility of *Satb1* was reduced in R+P, consistent with reduced transcription and its ability to repress PD-1 expression in $CD8^+$ T cells (52). Notably, increased chromatin accessibility in R and decreased in R+P T_{FGS} were also observed for T cell effector/memory genes, *Prf1, Ccl5, Ifngr1, FasL,* and *Gata3,* which were transcriptionally downregulated (Cluster D, Figure 3d) in post-partum memory T_{FGS} (Figure 6i-k, Extended Data Figure 10a-b) (29, 30, 48, 53).

Finally, HOMER *de-novo* motif analysis was used to search for enrichment of conserved transcription factor DNA binding motifs associated with T cell function and differentiation among the DAPs in R+P vs. R T_{FGS} (Extended Data Figure 11). This analysis identified in R+P vs. R T_{FGS}, key motifs closing for *Lef1, Tcf7, Tcf4, Tcfl2, Batf,* and motifs opening for *Nfatc1, Tbx21, Eomes, Runx,* and *Jun*, that have been implicated in T cell exhaustion (48). Together, these data support the conclusion of extensive epigenetic modification in post-partum memory T_{FGS} at loci involved in T cell exhaustion and in a subset of the memory T cell signature.

Pregnancy programs sustained hypofunction in memory T_{FGS}

Because T cell exhaustion is diminished upon antigen deprivation, we tested whether the exhaustion phenotype induced by pregnancy was persistent in P and R+P T_{FGS} (45, 54). On post-skin transplant (D30-60) or post-partum day 30-37, the expression of CD44 was significantly increased, and CD62L significantly reduced (Extended Data Figure 12a, b). The levels of exhaustion markers Tox, Tigit and PD-1 by R+P T_{FGS} remained significantly elevated compared to R or P T_{FGS} (Fig 7a). In contrast, the expression of, NFAT and FR4 was comparable in R+P and P T_{FGS}, while CD73 highest in P T_{FGS} (Fig 7a; Extended Data Figure 12c). These data suggest that pregnancy-induced exhaustion was persistent especially in post-partum memory compared to naive T_{FGS}.

We next quantified the in vitro cytokine production capability of $CD8^+$ T cells following stimulation with allogeneic APCs. As expected, ~12% and 30% of R T_{FGS} produced TNFα and IFNγ, respectively, which is significantly higher than N T_{FGS} (Fig 7b; Extended Data Figure 13). P T_{FGS} exhibited minimal TNFα and IFNγ production, remaining comparable to N T_{FGS}. Notably, TNFα production was significantly reduced in R+P T_{FGS} compared to R T_{FGS}, however, the ability to IFNγ was not significantly altered (Figure 7b).

Finally, we tested whether the recall encounter of fetal antigens by memory T cells during pregnancy resulted in a persistent hyporesponsive state in the context of offspring-matched heart transplantation. To avoid the humoral sensitization that is simultaneously elicited by pregnancy and that we have previously shown as sufficient to mediate rejection of F1-heart grafts (3), we used an adoptive transfer (AdTr) approach whereby $CD8^+$ T cells purified from R or R+P (post-partum day 0-10) mice were injected into naive B6 hosts. Following AdTr of $CD8^+$ T cells, B6 hosts were transplanted with an F1 heart graft (B6xBALB/c) and received anti-CD154 and donor splenocyte transfusion (DST) (anti-CD154/DST; Figure 1d-e), a therapy that induces long-term graft acceptance in naïve hosts. Consistent with previous reports (17, 18), memory $CD8^+$ T cells from R mice prevented stable graft acceptance. Remarkably, anti-CD154/DST treatment induced a significant extension of allograft survival in recipients of R+P $CD8^+$ T cells

(Figure 7c-d; Supplementary Table 2). Thus, pregnancy enforces a cell-intrinsic state of hypofunction in post-partum memory T_{FGS} that manifests as restored susceptibility to anti-CD154/DST-induced tolerance of offspring-matched heart grafts.

Discussion

Most studies of T cell tolerance to the semi-allogeneic fetus investigate the immunological effects of pregnancy in naive mice or those sensitized by prior pregnancy; in contrast, we show that the processes evoked during pregnancy are capable of restraining alloreactive memory T and B cell responses generated by skin graft rejection to allow for full-term delivery of viable semi-allogeneic offspring. The potential mechanisms mediating the reprogramming of memory $CD8^+$ T cells to hypofunction by pregnancy are suggested by their phenotypic and transcriptional signatures, which illustrated the differential impact pregnancy had on memory vs. naive T_{FGS}. Post-partum memory T_{FGS} had significantly higher transcriptional and phenotypic expression of exhaustion markers, Tox, Eomes, PD-1, and Tigit, whereas post-partum naive T_{FGS} preferentially expressed the anergy markers, FR4 and CD73. GSEA analysis confirmed that pregnancy-induced transcripts in R+P were significantly enriched for canonical $CD8^+$ T cell exhaustion signatures that were up- and down-regulated in $CD8^+$ T cells infiltrating tumors or in chronic infection. In contrast, P T_{FGS} were enriched for only upregulated transcripts associated with exhaustion. Additionally, even within the shared 196 DEGs induced by pregnancy in both naive and memory T_{FGS}, the magnitude of up- or downregulation was significantly greater in R+P compared to P T_{FGS}. We hypothesize that the higher levels of exhaustion and co-inhibitory markers are required to successfully restrain memory T cells, which have lower levels of activation thresholds due to increased TCR avidity and epigenetic programming (55, 56).

Changes in chromatin accessibility are the result of histone methylation, acetylation and phosphorylation that allow for increased or reduced transcriptional factor binding and subsequent gene transcription (57). We observed that pregnancy uniquely induced chromatin remodeling in memory $CD8^+$ T_{FGS}, whereas naive T_{FGS} remained largely epigenetically unmodified by pregnancy, even at shared exhaustion-associated loci induced transcriptionally by pregnancy. Additionally, pregnancy-induced opening of chromatin in post-partum memory T_{FGS} was enriched for transcription factor motifs implicated in both early- and late-stage T cell exhaustion, including *Tbx21*, *Eomes*, and *Jun* (48). These observations are congruent with the significant increase in transcription of exhaustion-associated genes in post-partum

memory T_{FGS}. That epigenetic modification enforces the hypofunctional state may provide an explanation for the resistance to NFAT inhibition seen in R+P compared to P T_{FGS}. The basis for why pregnancy has distinct chromatin remodeling effects in R+P vs. P T_{FGS} is unclear, but we speculate that it may be due to intrinsically distinct epigenetic landscape in N vs. R T_{FGS} from which R+P and P T_{FGS} are derived.

Our observations also support the hypothesis that the partial reduction of the memory transcriptome and epigenome contributes to the hypofunctional state of R+P T_{FGS}. In addition to the upregulation of DEGs negatively regulating cytokine production (*Havcr2*, *Pdcd1lg2*, *Tgfb3*), multiple genes involved in the rapid response upon antigen reencounter were downregulated in R+P vs. R T_{FGS}. These include genes encoding effector molecules (*CD48, Prf1, Fasl, Fcgr2b*, *Klr* family), chemokine/chemokine receptors (*Ccl6, Ccl9, Ccl5, Ccr2, Ccr3, Cxcr3, Cx3cr1, Xcr1*), and cytokine/ cytokine receptors (*Il18r1, Il18r1, Ifngr1, Il2rb*) (34, 45, 53, 55). Furthermore, a subset of these genes (*Ccl5, Gata3, Ifnr1, Prf1 and Fasl*) underwent chromatin remodeling following both rejection that was reversed by pregnancy. These data raise the tantalizing possibility that pregnancy utilizes targeted epigenetic modifications in memory T_{FGS} not only to induce transcriptional exhaustion but also to dedifferentiate T_{FGS} from memory/effector programming.

Memory $CD8^+$ T_{FGS} generated following rejection of allogeneic skin grafts exhibit increased production of TNFα and IFNγ and resistance to co-stimulation blockade-mediated acceptance of heart allografts compared to naive T_{FGS} (3, 16-18). Post-partum memory $CD8^+$ T cells exhibited significantly reduced ability to produce TNFα, but retained their ability to produce IFNγ, relative to R $CD8^+$ T cells. The physiological roles of uterine NK cells producing IFNγ in promoting pregnancy, vascular/tissue remodeling and preventing excessive trophoblast invasion have been described (58, 59). Furthermore, TNFα combined with high doses of IFNγ is compatible with healthy pregnancy, and "controlled" levels of Th1 cells and TNFα may have essential roles in successfully pregnancy (58, 60, 61). Thus, we speculate that the ability to produce IFNγ and TNFα by T cells may be preserved in pregnancy. It is notable that IFNγ plays a non-redundant role in allograft tolerance, as mice deficient in IFNγ fail to develop tolerance with no defects in acute rejection (62, 63). Indeed, we show that pregnancy was able to relieve the barrier memory $CD8^+$ T cells normally pose to transplantation tolerance, as evidenced by the enhanced survival of

subsequent offspring-matched heart grafts under co-stimulation blockade in recipients that received R+P vs. R $CD8^+$ T_{FGS} cells. These observations provide proof-of-concept that memory $CD8^+$ T cells, which heretofore were considered an insurmountable barrier to clinical transplantation tolerance, can be reprogrammed to hypofunction and susceptibility to anti-CD154/DST-induced graft acceptance.

There are several limitations to this study. Firstly, we introduced a model OVA antigen to the semi-allogeneic fetus and allograft to enable tracking endogenous polyclonal fetus/graft specific $CD8^+$ T cells. It is possible that the highly immunogenic OVA may be immunodominant over “true” alloantigens and elicit higher avidity T cell responses than observed for alloreactive T cells. Secondly, our data suggest that the expression of exhaustion transcriptome and markers, as well as the partial reversal of the memory phenotype contributes to the hypofunctional state of post-partum memory T_{FGS}. However, definitive necessity and sufficiency studies are necessary. Thirdly, a mechanistic explanation for why memory but not naive T_{FGS} undergo such extensive chromatin remodeling during pregnancy is lacking, and necessity of this remodeling for the maintenance of the hypofunction state in post-partum memory T_{FGS} has not be demonstrated. Finally, while sensitivity to co-stimulation blockade is significantly restored, all the F1 heart grafts ultimately rejected. Post-partum memory T_{FGS} retained the ability to produce IFNγ and TNFα, and a subset of R T_{FGS} were unmodified by pregnancy. These observations suggest that additional memory programs have to be constrained to achieve comparable states of hypofunction as observed in post-partum naive T_{FGS} (3).

Pregnancy is an immunological paradox, wherein the conflict between the preservation of robust immunity towards foreign pathogens and tolerance to the semi-allogeneic fetus must be simultaneously resolved to preserve the survival of the species. Furthermore, memory fetus-specific T cells must be constrained. The imperative to preserve fetal viability underscores the necessity of multiple conserved and redundant mechanisms for controlling both naïve and memory T cells. Our studies reveal a potentially novel endogenous mechanism for the reprogramming of antigen-specific memory T cells towards exhaustion and hypofunction (Extended Data Figure 14). This mechanistic insight is critically relevant for understanding semi-allogeneic pregnancy as well as the successful induction of transplantation tolerance

in the clinic, where no conceptual framework for reprogramming of memory donor-specific T cells has yet been identified (16-18). In addition, viewing $CD8^+$ T cell exhaustion/hypofunction through the lens of pregnancy potentially solves the seemingly counterintuitive evolutionary puzzle of why exhaustion is so quickly induced when T cells are exposed to chronic infections or tumors, which is often detrimental to the host (64). We theorize that this timeline is imposed by mammalian pregnancy requiring a rapid restraint of fetus-specific alloreactive T cells to preserve fetal viability. Moreover, while the phenotype and transcriptome of exhaustion was initially discovered in the context of chronic infection and tumors, we posit that this phenomenon should be re-evaluated from the perspective that exhaustion pathways developed due to the stringent need to preserve the semi-allogeneic fetus, and these mechanisms have been subsequently hijacked by chronic infections and tumors. Thus, insights into how exhaustion is programmed into memory T_{FGS} during pregnancy are relevant not only to addressing problems related to high-risk pregnancies and transplantation tolerance, but also to broader clinical issues such as autoimmunity, chronic infection, and cancer, where controlling T cell hypofunction is also desirable.

Methods

Sex as a biological variable: This study's main focus is the effect of pregnancy on the maternal immune system. The investigation of pregnancy justifies and necessitates the use of exclusively female mice in this study.

Mice. Eight- to twelve-week-old female C57Bl/6 (B6, H-2^b) mice were purchased from Harlan Laboratories. *Act-2W-OVA* transgenic mice on a B/6 background (2W-OVA.C57BL/6) were a gift from James Moon (Massachusetts General Hospital, Harvard Medical School, Charlestown, Massachusetts, USA). Donor/paternal 2W-OVA.BALB/c (2W-OVA.B/c, H-2^d) mice were backcrossed from 2W-OVA.B/6 mice for >10 generations. For semi-allogeneic pregnancies, a harem breeding involving one male 2W-OVA.BALB/c with 4 virgin or post-partum B/6 females. Approximately 50% of F1 from this mating were confirmed to be 2W-OVA-positive, and 2W-OVA.F1 (B6x2W-OVA.B/c) mice were used as heart donors.

Adoptive transfer, heart, and skin transplantation. For adoptive transfer experiments, ~4-12x10^6 CD45.2^+ $CD8^+$ T cells, isolated via magnetic enrichment, were transferred retro-orbitally (r.o.) into naive CD45.1^+ C57BL/6 hosts one day prior to heart transplantation. See below for T cell enrichment description. Heterotopic heart transplantations were performed as previously described (65), by grafting 2W-OVA.F1 (B6x2W-OVA.B/c) hearts onto the inferior vena cava and aorta of female recipients. Tolerance (CoB/DST) was induced with a combination of anti-CD154 (MR1, BioXCell) at a dose of 500μg on day 0 (i.v.), and 250μg on days 7 and 14 (i.p.) post-transplantation, in combination with 2x10^7 donor spleen cells on day 0. Graft survival was assessed by palpation 2-3 times per week, and the day of rejection was defined as the last day of detectable heartbeat. Flank skin from 2W-OVA.BALB/c was transplanted onto the B/6 mice.

FK506 injection. FK506 was injected daily (1 mg/kg i.p.) into pregnant mice beginning 5 days after the first observation of a copulation plug and ending on the date of euthanasia (day 0-3 post-delivery).

T Cell enrichment. Single-cell suspensions from spleens and pooled LNs (brachial, inguinal, and axillary) of individual mice were prepared for each experiment (see below). For flow cytometry and cell sorting assays, Pan-T lymphocytes were enriched with Pan-T cell isolation kit II (Miltenyi Biotech). For $CD8^+$ T cell adoptive transfer experiments, the $CD8\alpha^+$ T Cell isolation kit (Miltenyi Biotech) was used instead. Samples were passed through LS columns on a QuadroMACS separator (Miltenyi Biotech) in MACS buffer (2%FBS + 2mM EDTA)

Cell harvest and fluorescent staining for flow cytometry and cell sorting. Spleens and LNs were harvested and passed through a 40μm cell strainer (Corning Inc., USA), followed by lysis of red blood cells via 2-minute incubation with ammonium chloride-potassium (ACK) lysis buffer (Quality Biological). After magnetic enrichment for T cells (see above), approximately $2x10^7$ cells were stained with a fixable live/dead stain (Invitrogen), followed by tetramer staining. Tetramer staining was performed for 35-45 min at room temperature with PE- and APC-conjugated OVA (SIINFEKL):H-$2K^b$ tetramers (NIH Tetramer Core Facility). The cells were then stained for extracellular antibodies for 15-20min at 4°C. Samples were fixed with the Invitrogen Fix/Perm buffer kit according to the manufacturer's instruction. Finally, fixed and permeabilized samples were stained for intracellular markers overnight. For phenotypic analysis, samples were acquired via flow cytometry after fixation and intracellular staining. For cell sorting, samples were sorted into RPMI after extracellular staining.

In vitro stimulation and staining for IFNγ and TNFα. Splenocyte stimulators from 2W-OVA.F1 mice were treated with ACK lysing buffer (Quality biological), followed by 30min incubation with anti-CD90.2 (53-2.1, BD Biosciences) to deplete T cells. Labeled T cells were depleted with two consecutive 35min incubations with rabbit complement (Cedarlane) at 37°C, and then incubated overnight with 20μg/ml LPS. 1×10^6 responder cells (Pan-T enriched splenocytes) were plated with 0.5×10^6 stimulators (T-depleted APC's) in triplicate in a 96-well plate (Corning) and incubated at 37°C overnight. Next, Golgi Plug (BD Biosciences) was added at 1:1000 and incubated for an additional 6h at 37°C. Live/Dead and extracellular staining were performed for 10min and 15min (respectively) on ice, and cells were then fixed with BD

Cytofix/Cytoperm according to the manufacturer's instruction (BD Biosciences). Finally, cells were stained for intracellular IFNγ and TNFα and acquired via flow cytometry.

Flow cytometry and cell sorting acquisition and analysis. Flow cytometry samples for phenotypic panels and in-vitro cytokine stimulation assays were acquired on a Cytek Aurora flow cytometer (5 lasers, 16UV-16V-14B-10YG-8R). For cell sorting, samples were acquired and sorted on a BD Aria II 4-15 (70μm nozzle), BD Aria Fusion 5-18 (70μm nozzle), or the Invitrogen Bigfoot (100μm nozzle). The associated software for each cytometer is as follows: Aurora is Cytek SpectroFlo, Aria and Aria Fusion are BD FACSDiva, and Bigfoot is Invitrogen Sasquatch Software (SQS). Data were analyzed and visualized with FlowJo software v10.8.1 (FlowJo, LLC).

Fluorescent antibodies for flow cytometry and cell sorting. Fluorochrome-conjugated antibodies were used to select and sort cell subsets, analyze T cell phenotypes, and to determine cytokine production. The following antibodies were used in this study, separated by manufacturer (clone is indicated in parentheses). *Biolegend:* Ki67-PacificBlue (16A8), CD62L-BV510 (MEL-14), CD73-BV605 (TY/11.8), CD44-FITC (IM7), PD1-PEDazzle594 (RMP1-30), TIGIT-PECy7 (1G9), LAG3-BV785 (C9B7W), IFNγ (XMG1.2), TNF-α-PECy7 (MP6-XT22), SATB1-AlexaFluor594 (O96C6), TIM3-APC/Fire750 (B8.2C12), OX40-BV711 (OX-86), OX40L-PECy7 (RM134L), Tim3-PerCP/Cy5.5 (B8.2C12), CD8-FITC (53-6.7), CD90.2-PECy7 (30-H12), CD90.2-PerCP/Cy5 (53-2.1), CD4-APCCy7 (RM4-5). || *BD Biosciences:* CD90.2-BUV395 (53-2.1), CD4-BUV496 (GK1.5), CD19-BUV661 (1D3), CD11c-BUV661 (N418), F4/80-BUV661 (T45-2342), NK1.1-BUV661 (PK136), TER119-BUV661 (TER-119), CD127-BUV737 (SB/199), CD8-BUV805 (53-6.7), FR4-BV421 (12A5), CTLA4-APCR700 (UC10-4F10-11), NK1.1-eFluor450 (PK136), Ter-119-eFluor450 (Ter-119), Rorγt-BV650 (Q31-378), CD62L-BV605 (MEL-14). || *Invitrogen:* FoxP3-AlexaFluor532 (FJK-16s), CD44-BUV737 (IM7), PD1-SB780 (J43), TOX-eFluor660 (TXRX10), EOMES-PerCP/eFluor710 (Dan11mag), F4/80-eFluor450 (BM8), CD49b-eFluor450 (DX5), CD11c-eFluor450 (N418), PD1-PerCP-e710 (J43). || *Santa Cruz Biotechnologies:* NFATc1-AlexaFluor488 (7A6), CD30L-AlexaFluor680 (RM153).

RNA-Sequencing Data Collection and Processing. RNA-Seq libraries were generated and amplified according to the SmartSeq2 protocol (66). 200 live cells per sample/subset were sorted into 96-well optical PCR plates (Thomas Scientific) containing 4µl of lysis buffer at 4°C. cDNA sequencing libraries were generated using Nextera XT DNA Library Prep Kit and Nextera XT Index Kit (Illumina). All libraries were sequenced in the same run on a NovaSeq 6000 in a 150 bp/150 bp paired-end configuration. An average of ~55 × 10^6 paired reads was generated per sample.

RNA-Sequencing Data and Processing. Raw RNA-Seq reads were trimmed for adapter content and filtered for truncated reads using Cutadapt v3.4 (67). Paired-end reads were aligned using STAR v2.6.1b (68) against the GRCm39 (mm39) reference genome and transcriptome annotations, and non-uniquely mapping reads were removed. Per-sample read counts for each gene were quantified sample using featureCounts v2.0.1 (69).

ATAC sequencing. Chromatin profiling was performed by ATAC-seq as described previously (70, 71). In brief, ~3,000-50,000 sorted cells were washed in cold PBS and lysed to isolate intact nuclei. Transposition was performed at 37°C for 30min with the Tagment DNA Enzyme and Buffer kit (Illumina). After purification of the transposed DNA with the MinElute PCR purification kit (Qiagen), material was amplified via PCR for 13-14 cycles with Nextera XT Index primers (Illumina). Final product was purified again via MinElute PCR purification kit (Qiagen). Libraries were sequenced in the same run on a NovaSeq 6000 in a 150 bp/150 bp paired-end configuration. An average of 75 × 10^6 paired reads was generated per sample.

ATAC-Sequencing Data and Processing. Raw ATAC-Seq reads were trimmed for adapter content and filtered for truncated reads using Cutadapt v3.4 (67). Paired-end reads were aligned using Bowtie2 v2.2.9 (72) against the GRCm39 (mm39) reference genome. Non-uniquely mapping reads and PCR duplicates were filtered with Bamtools v2.5 and Picard v2.21.8, respectively (73, 74). Peaks corresponding to ATAC-Seq cut sites for each sample were called using Genrich v0.6.1 in ATAC-Seq mode (https://github.com/jsh58/Genrich). Finally, reproducibly identifiable peaks for each experimental group were identified via ChIP-R v1.2.0 (75).

Processing of ATAC-Seq peak set for differential accessibility analysis. Reproducibly identifiable peaks across all experimental groups were merged into a single reference peak set using Bedtools v2.27.1 (76). Multibamsummary v3.5.1 from the Deeptools suite (77) was used to generate per-sample read counts at each peak from the reference peak set. The read counts data was then imported into R v4.1.0, and each peak was assigned to a single gene via nearest TSS using GenomicRanges v1.46.1, ChIPpeakAnno v3.28.1, and the Org.mm.eg.db v3.14.0 genomic annotation object (78, 79).

Sequencing Data Analysis and Visualization. After completing data preprocessing as described above, the DESeq v1.34.0 package was used to conduct differential expression/accessibility analysis on sequencing datasets (80). For both RNA-Seq and ATAC-Seq, the threshold for determining differential expression/accessibility was FDR (p_{adj})<0.1 and absolute value of $\log_2$ fold-change >0.9. In addition to DESeq2, we used current versions of the following packages for analysis and visualization (with description of purpose in parentheses). Viridis and RColorBrewer (color scale creation). Gplots, ggplot2 and ggrepel (graphing data and generating heatmaps). Uwot and VennDiagram (UMAP and Venn graphs, respectively). Tidyverse suite (dataset manipulation).

ATAC-Seq motif analysis and locus visualization. Motif analysis was performed by identifying unique and common peak sets between two experimental groups (using the reproducible peaks for each group as described above). These peak sets were then analyzed via HOMER de-novo motif analysis (81) to search for significantly enriched motifs associated with ATAC-Seq cut sites and annotate these motifs to possible transcription factor targets. Individual loci were visualized by generating bigwig files for each sample and importing them into IGV v2.12.3 (82). A single track for each experimental group was created by summing the read counts of two representative samples from each group.

Gene Set Enrichment Analysis. GSEA software (4.0.3) was downloaded from the Broad Institute (https://www.gsea-msigdb.org/gsea/index.jsp), and pre-ranked GSEA was performed on the selected gene sets in this study. Gene set files were downloaded from the Molecular Signatures Database or prepared manually as gene matrix expression files (.GMX), using DESeq2 on published RNA-Seq data. Ranked

gene lists for our transcriptional data were generated from by arranging genes based on the Change Metric (fold change × $-\log_{10} p_{adj}$) from high to low. The change metric combines both significance and intensity of expression changes, while preserving the direction (up- or -downregulation) with positive or negative values.

Pathway Analysis. Two lists of DEGs (or differentially accessible peaks) were created for each pairwise comparison, one for upregulated/opened regions, and one for downregulated/closed regions. The ENSEMBL gene IDs of each list were then uploaded to Metascape Pathway analysis (83) to calculate the enrichment and significance of functional gene pathways from Gene Ontology (GO), Kegg, Reactome, or WikiPathways databases (primarily GO).

Computational resources. All data preprocessing for both ATAC-Seq and RNA-Seq (adapter trimming, alignment, filtering, generation of read-counts, and peak-calling) was performed on the Midway2 high-performance compute cluster, which is maintained by the University of Chicago Research Computing Center.

Statistics. Statistical significance analyses were performed using GraphPad Prism version 9.2.0. Sample size of >5 animals per experiment were chosen to ensure adequate power. Graft survival significance was assessed using a Kaplan-Meier/Mantel-Cox log rank test. *P* values <0.05 were considered to indicate a significant difference. To calculate differences between experimental animals, we used Kruskal-Wallis test (ANOVA) with Dunn's post hoc test for pairwise multiple comparisons, one-way ANOVA with Tukey's post-hoc test, or Welch's unpaired *t* test (specific tests for each subfigure are indicated in the figure legends). Asterisks used to indicate significance correspond to the following: **p*<0.05, ***p*<0.01, ****p*<0.001, and *****p*<0.0001.

Study approval: All animal experiments were approved by the Institutional Animal Care and Use Committee at the University of Chicago and adhered to the standards of the NIH Guide for the Care and Use of Laboratory Animals.

Data availability: The RNA-seq and ATAC-seq data have been deposited as a SuperSeries in the Gene Expression Omnibus (Accession code GSE216302). All scripts used for data analysis have been uploaded to GitHub at https://github.com/jardplard/Chong_CD8_Pregnancy. This repository includes the supporting data values for additional graphs displayed in this manuscript that were not generated from the scripts mentioned above ("Merged Source Data.xls"). Additional information and materials will be made available upon request.

Code availability: All code was generated based on publicly available software packages; scripts used for data analysis have been uploaded to GitHub at https://github.com/jardplard/Chong_CD8_Pregnancy..

Conflict of interest: The authors have declared that no conflict of interest exists.

Author Contributions: Authorship order was made after discussion between co-first and co-senior authors, with additional recommendation from three anonymous faculty at the University of Chicago. JMP designed and performed the experiments and analyzed data, including pipeline design and script writing for ATAC-Seq and RNA-Seq preprocessing and downstream analyses. JMP wrote the manuscript and generated figures, with guidance from ASC and MLA. GH also performed experiments that generated flow cytometry data, and analyzed RNA-seq and ATAC-seq data, generated figures, and edited the manuscript. DY and ASC conceived the initial project, and DY performed skin and heart transplantations. MM and FG provided supervision on ATAC-Seq and integrated bioinformatics analysis. All authors provided feedback on figure layout and manuscript content.

Acknowledgments: This work was supported in part by grants (R01AI142747, P01AI097113) from the National Institute of Allergy and Infectious Diseases (NIAID), National Institutes of Health. MHC tetramers were provided by the NIH Tetramer Core Facility (contract HHSN272201300006C). We also thank the Cytometry and Antibody Technology (flow cytometry) core, which receives financial support from the Cancer Center Support Grant (P30CA014599); RRID: SCR_017760. Finally, we thank the Animal

Resources Center at The University of Chicago for their assistance. The T_{EX} datasets used for GSEA analysis were generously provided by Dr. Paige Porrett (University of Alabama, Birmingham, AL) (6).

Figures and Legends

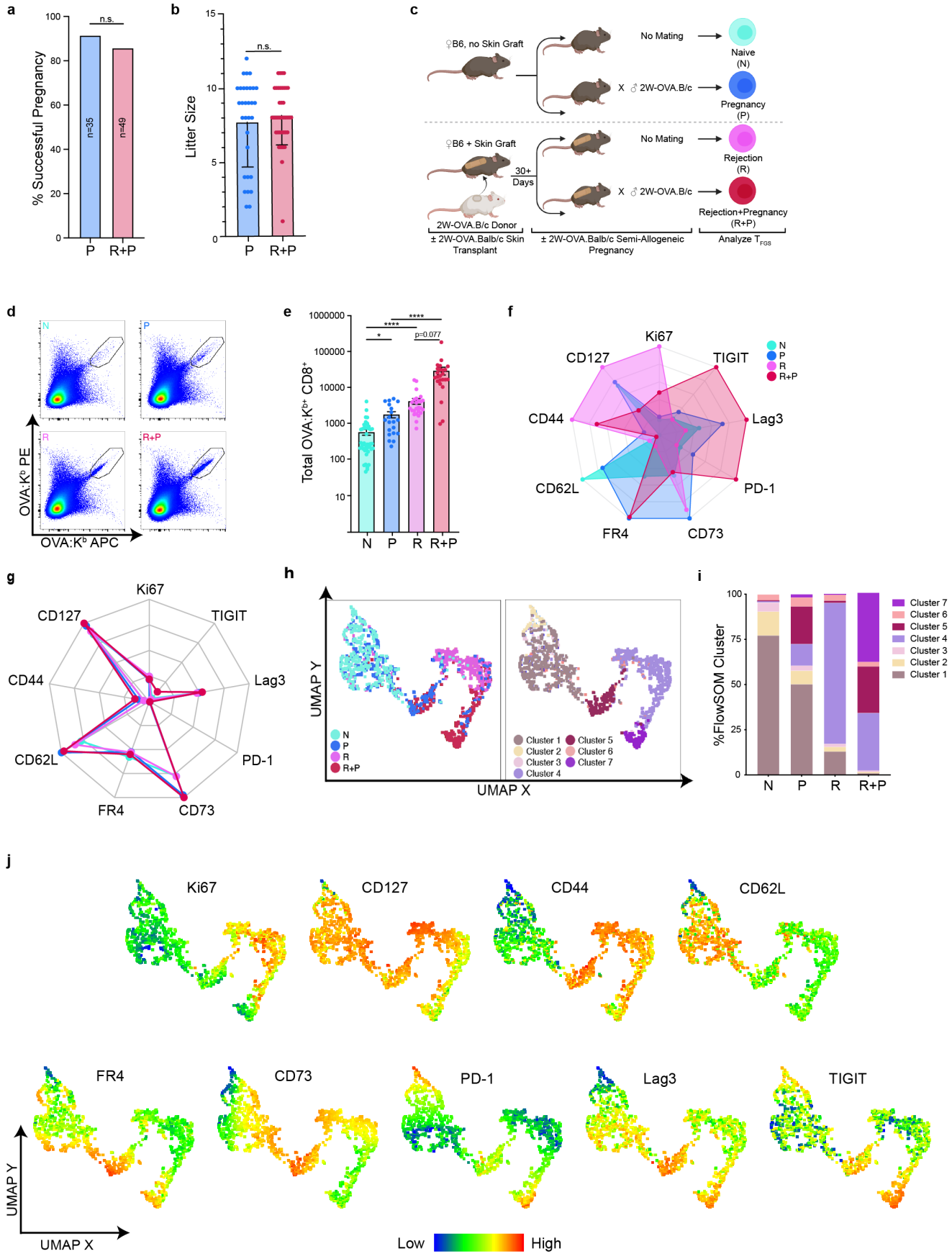

Figure 1: Pregnancy induces a hypofunctional phenotype in memory OVA-specific T_{FGS}. a, Bar graph showing percentage of Naive vs. Sensitized female mice achieving successful full-term pregnancies; *n* = 35-49 mated mice per group. Additionally, there was a 100% success rate in sensitized mice subjected to a second pregnancy (*n*=12). P values were determined by Chi-square (χ^2) Test of Independence. **b,** Bar graph showing number of viable pups at birth (litter sizes) of Naive vs. Sensitized female mice achieving successful full-term pregnancies; *n* = 31-39 per group. Each dot indicates individual mice. **c,** Experimental design. Female B6 mice were mated with transgenic 2W-OVA.B/c mice, with or without sensitization to 2W-OVA.B/c via skin graft 30 days prior (R+P and P, respectively). Unmated mice with or without skin graft rejection were included as controls (naïve (N) and rejection (R), respectively). **d,** Representative pseudocolor plots showing OVA:K^b-specific $CD8^+$ T cells (T_{FGS}). Each dot indicates individual mice. **e,** Normalized total recovery of T_{FGS} cells at post-partum day 0-3. Data acquired from 2 or more biologically independent experiments; *n* = 20-38 per group. P values were determined by Kruskal-Wallis test with Dunn's post hoc test. **f-g**, Radar plot showing phenotypic profile of (f) T_{FGS} or (g) non-T_{FGS} based on markers of activation, memory, and co-inhibition. Data are normalized to the highest and lowest MFI for each marker expressed by T_{FGS} or non-T_{FGS} from all 4 experimental groups. Symbols color coded as in d. Expression is represented as normalized percentage of the highest/lowest-expressing group (based on all OVA^+T_{FGS} and non- T_{FGS}) for each marker. **h**, UMAP with experimental groups (left) and FlowSOM clustering (right) reveals distinct phenotypic subsets in T_{FGS}. **i**, Stacked bar graph showing FlowSOM cluster distributions for each experimental group. **j**, UMAP with heatmap overlays to show expression of each phenotypic marker on T_{FGS} at single-cell resolution. Data represent mean ± SEM. Gating strategy, statistical analysis and representative histograms of this flow dataset are in Extended Data Figure 1a-c. ns: not significant; *P<0.05; ****P<0.0001.

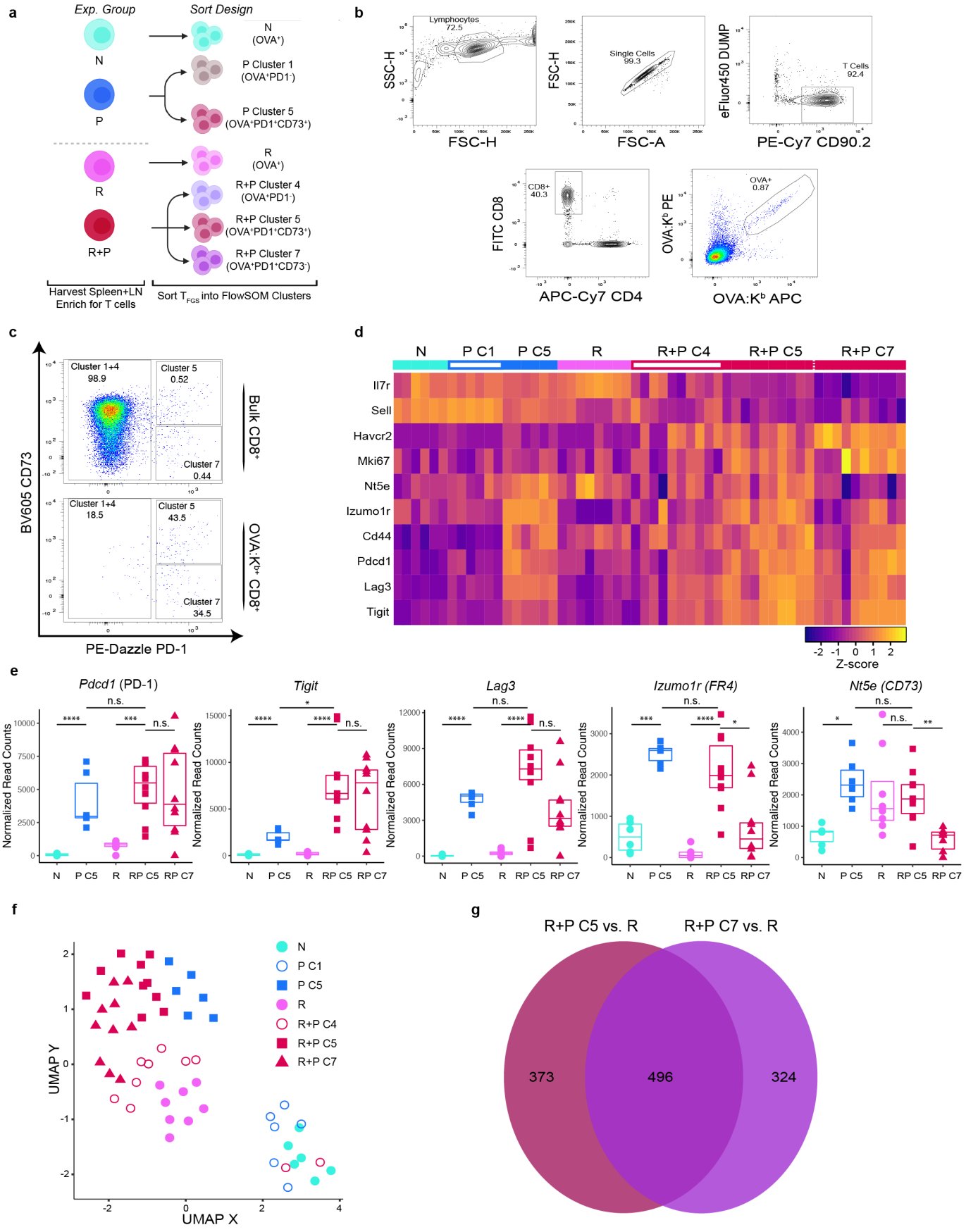
a
Exp. Group
Sort Design
N
P
R
R+P
N (OVA+)
P Cluster 1 (OVA+PD1-)
P Cluster 5 (OVA+PD1+CD73+)
R (OVA+)
R+P Cluster 4 (OVA+PD1-)
R+P Cluster 5 (OVA+PD1+CD73+)
R+P Cluster 7 (OVA+PD1+CD73-)
Harvest Spleen+LN Enrich for T cells
Sort T FGS into FlowSOM Clusters
b
Lymphocytes 72.5
SSC-H
FSC-H
Single Cells 99.3
FSC-H
FSC-A
T Cells 92.4
eFluor450 DUMP
PE-Cy7 CD90.2
CD8+ 40.3
FITC CD8
APC-Cy7 CD4
OVA+ 0.87
OVA:Kb PE
OVA:Kb APC
c
Cluster 1+4 98.9
Cluster 5 0.52
Cluster 7 0.44
Bulk CD8+
Cluster 1+4 18.5
Cluster 5 43.5
Cluster 7 34.5
OVA:Kb+ CD8+
BV605 CD73
PE-Dazzle PD-1
d
N
P C1
P C5
R
R+P C4
R+P C5
R+P C7
Il7r
Sell
Havcr2
Mki67
Nt5e
Izumo1r
Cd44
Pdcd1
Lag3
Tigit
Z-score
e
Pdcd1 (PD-1)
Tigit
Lag3
Izumo1r (FR4)
Nt5e (CD73)
Normalized Read Counts
n.s.
N
P C5
R
RP C5
RP C7
f
UMAP Y
UMAP X
N
P C1
P C5
R
R+P C4
R+P C5
R+P C7
g
R+P C5 vs. R
R+P C7 vs. R
373
496
324

1

Figure 2: Pregnancy induces broad transcriptional modification in memory OVA-specific T_{FGS}. a, Sorting strategy for OVA:K^b-specific T_{FGS} from each experimental group into their most prevalent phenotypic subsets as defined by FlowSOM (in **Fig 1i**). T_{FGS} were acquired and sorted from 2 biologically independent experiments; *n* = 3-5 per group, with technical replicates for each biological sample. **b,** Gating strategy for each cluster of OVA:K^b-specific T_{FGS}. **c,** Representative plots showing the distributions of Cluster 1+4, Cluster 5, and Cluster 7 within bulk or OVA:K^b-specific R+P $CD8^+$ T cells. Percentage of each cell cluster is comparable to the distribution of our FlowSOM analysis in Figure 1h for the experimental groups. **d-e,** Row-normalized RNA-seq expression and box plots of normalized RNA-seq read counts for key exhaustion and anergy markers corresponding to **Fig 1i**. Each dot in box plots or UMAP, and each column in the heatmap, indicates individual mice. P values (in **e**) were determined by Kruskal-Wallis test with Dunn's post hoc test. ns: not significant; *P<0.05; ***P<0.001; ****P<0.0001. **f,** UMAP comparing all T_{FGS} subsets analyzed by RNA-seq. **g,** Venn diagram of DEGs unique to R+P C7 T_{FGS}, R+P C5 T_{FGS}, and shared between both subsets.

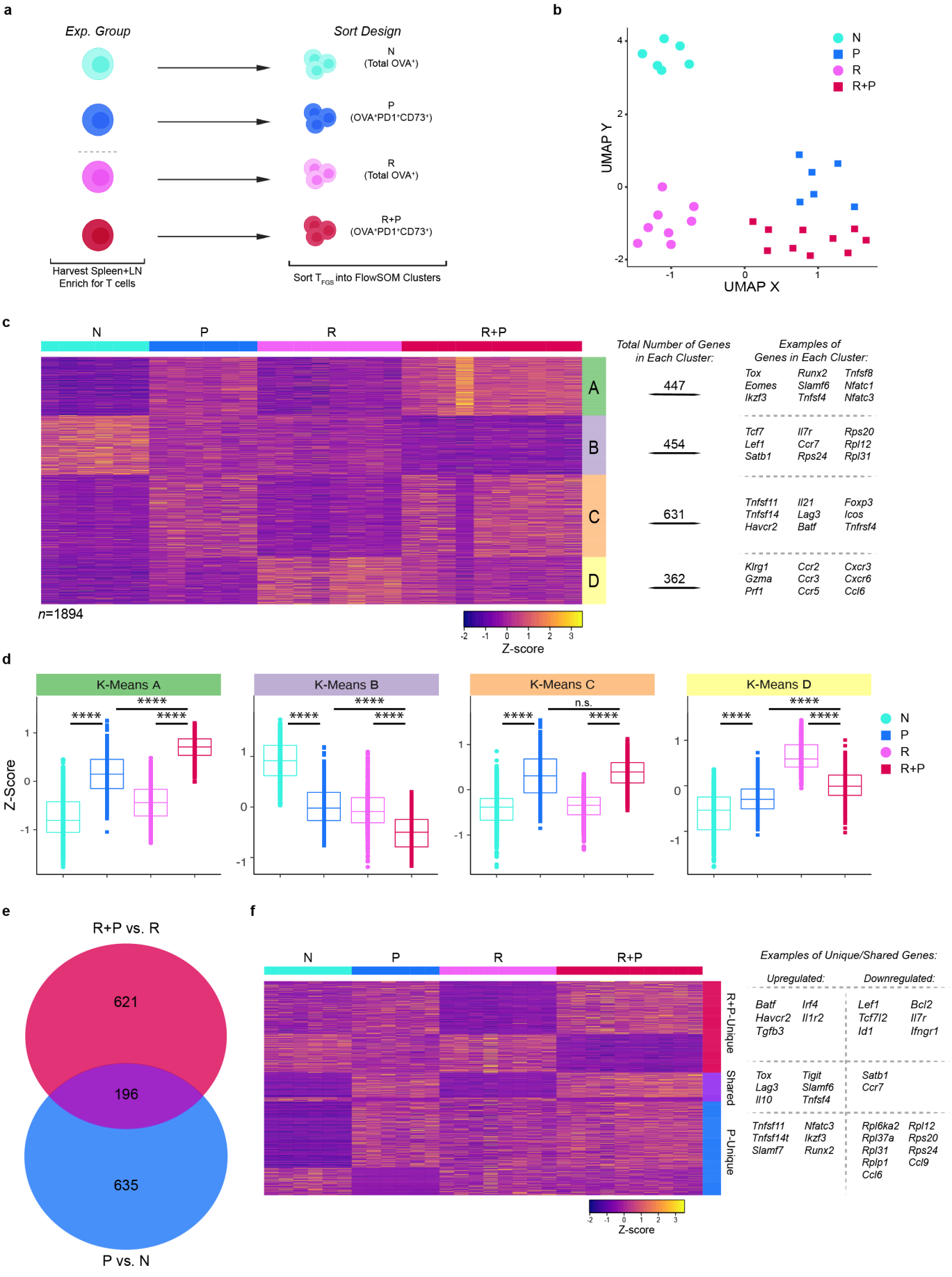
a
Exp. Group
Sort Design
N
(Total OVA+)
P
(OVA+PD1+CD73+)
R
(Total OVA+)
R+P
(OVA+PD1+CD73+)
Harvest Spleen+LN
Enrich for T cells
Sort TFGS into FlowSOM Clusters
b
UMAP Y
UMAP X
N
P
R
R+P
c
N
P
R
R+P
A
B
C
D
n=1894
Z-score
Total Number of Genes in Each Cluster:
447
454
631
362
Examples of Genes in Each Cluster:
Tox Runx2 Tnfsf8
Eomes Slamf6 Nfatc1
Ikzf3 Tnfsf4 Nfatc3
Tcf7 Il7r Rps20
Lef1 Ccr7 Rpl12
Satb1 Rps24 Rpl31
Tnfsf11 Il21 Foxp3
Tnfsf14 Lag3 Icos
Havcr2 Batf Tnfrsf4
Klrg1 Ccr2 Cxcr3
Gzma Ccr3 Cxcr6
Prf1 Ccr5 Ccl6
d
K-Means A
K-Means B
K-Means C
K-Means D
Z-Score
****
n.s.
N
P
R
R+P
e
R+P vs. R
621
196
635
P vs. N
f
N
P
R
R+P
R+P-Unique
Shared
P-Unique
Z-score
Examples of Unique/Shared Genes:
Upregulated:
Downregulated:
Batf Irf4
Havcr2 Il1r2
Tgfb3
Lef1 Bcl2
Tcf7l2 Il7r
Id1 Ifngr1
Tox Tigit
Lag3 Slamf6
Il10 Tnfsf4
Satb1
Ccr7
Tnfsf11 Nfatc3
Tnfsf14t Ikzf3
Slamf7 Runx2
Rpl6ka2 Rpl12
Rpl37a Rps20
Rpl31 Rps24
Rplp1 Ccl9
Ccl6

1

Figure 3: Post-partum memory and naive OVA-specific T_{FGS} acquire distinct and shared transcriptional signatures. a. OVA:K^b-specific T_{FGS} from each experimental group; N, R, P (C5) and R+P (C5) **b**, UMAP plot comparing transcriptional profiles among T_{FGS} subsets. **c-d,** Row-normalized RNA-seq expression of the top differentially expressed genes (*n*=1894) (**c**), organized by K-means clustering into Clusters A-D, indicated by right-side column. The total number and examples of DEGs in each K-means cluster are listed on the right. **d**, Box plots visualizing relative expression of DEGs in each K-Means cluster identified in (**c**). Minimum criteria for DEGs shown in this figure was both q<0.1 and $\log_2$ fold-change>0.9. P values (in **d**) were determined by Kruskal-Wallis test with Dunn's post hoc test. ns: not significant; ****P<0.0001. **e.** Venn diagram and **f**, row-normalized RNA-seq expression of DEGs induced by pregnancy in only R+P (n=635 DEGs), only P (n=621 DEGs) or both R+P and P T_{FGS} (n=196 DEGs). Each dot in UMAP or box plots, and each column in the heatmap, indicates individual mice.

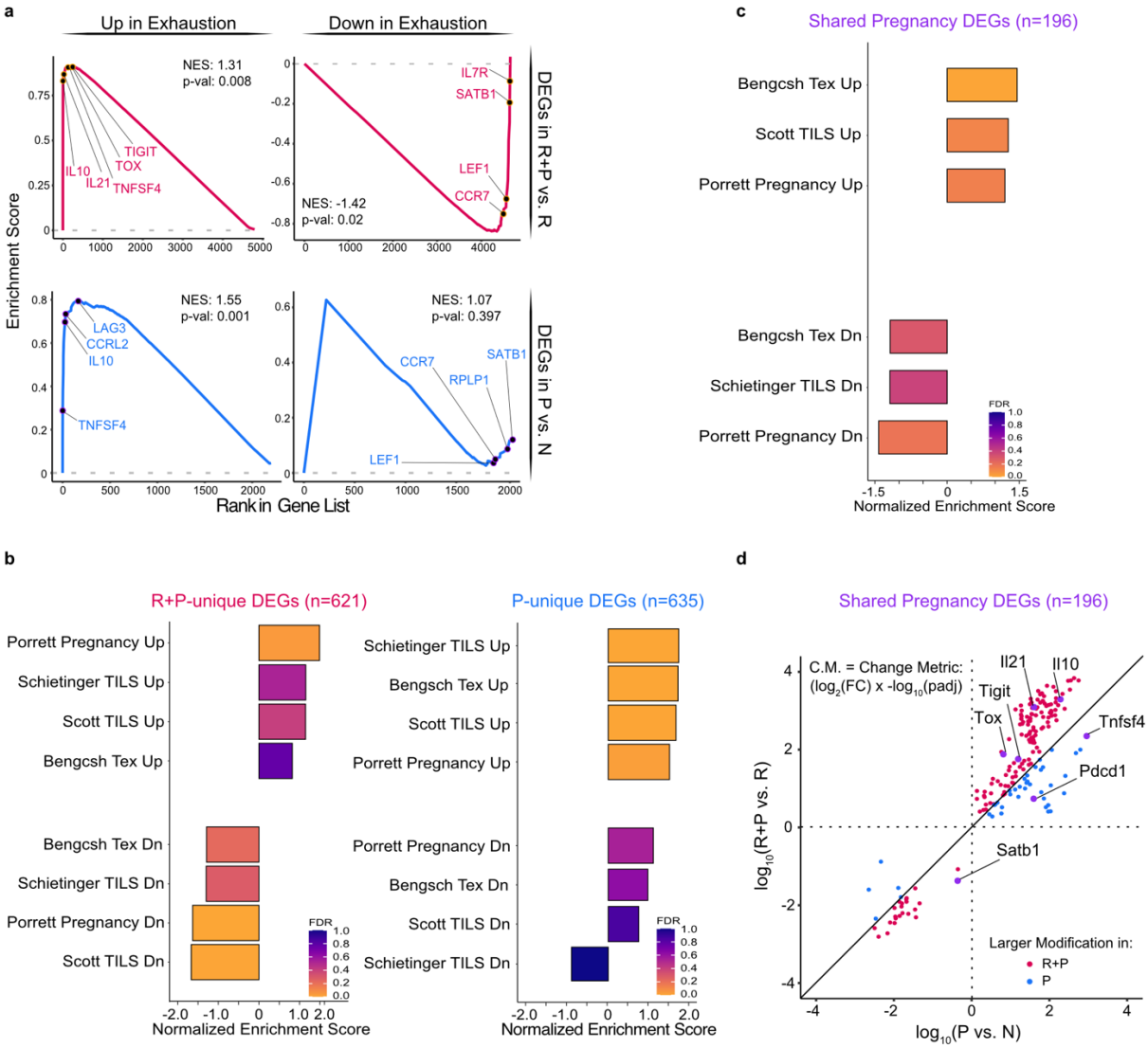

Figure 4: Post-partum memory OVA-specific T_{FGS} acquire a transcriptional signature of exhaustion. a, GSEA curves showing enrichment of the exhausted T cell signature (chronic viral infection (38)) in R+P vs. R and P vs. N DEGs. NES, Normalized Enrichment Score. **b**, Summary of GSEA analysis comparing DEGs unique to R+P vs. R (left) or P vs. N (right) or **c,** shared DEGs by R+P and P to published gene sets of exhaustion (6, 38-40). **d**, Dot plot comparing magnitude of up- or downregulation for shared DEG's between R+P and P T_{FGS} using the Change Metric (C.M.), a single statistic that merges FDR-corrected p-value and log fold change ($\pm\log_2$(FC) x -log(FDR)). P-values were calculated with the Wilcoxon matched-pairs signed rank test comparing R+P vs. P T_{FGS}. P(upregulation)<0.0001 | P(downregulation)=0.0032 |.

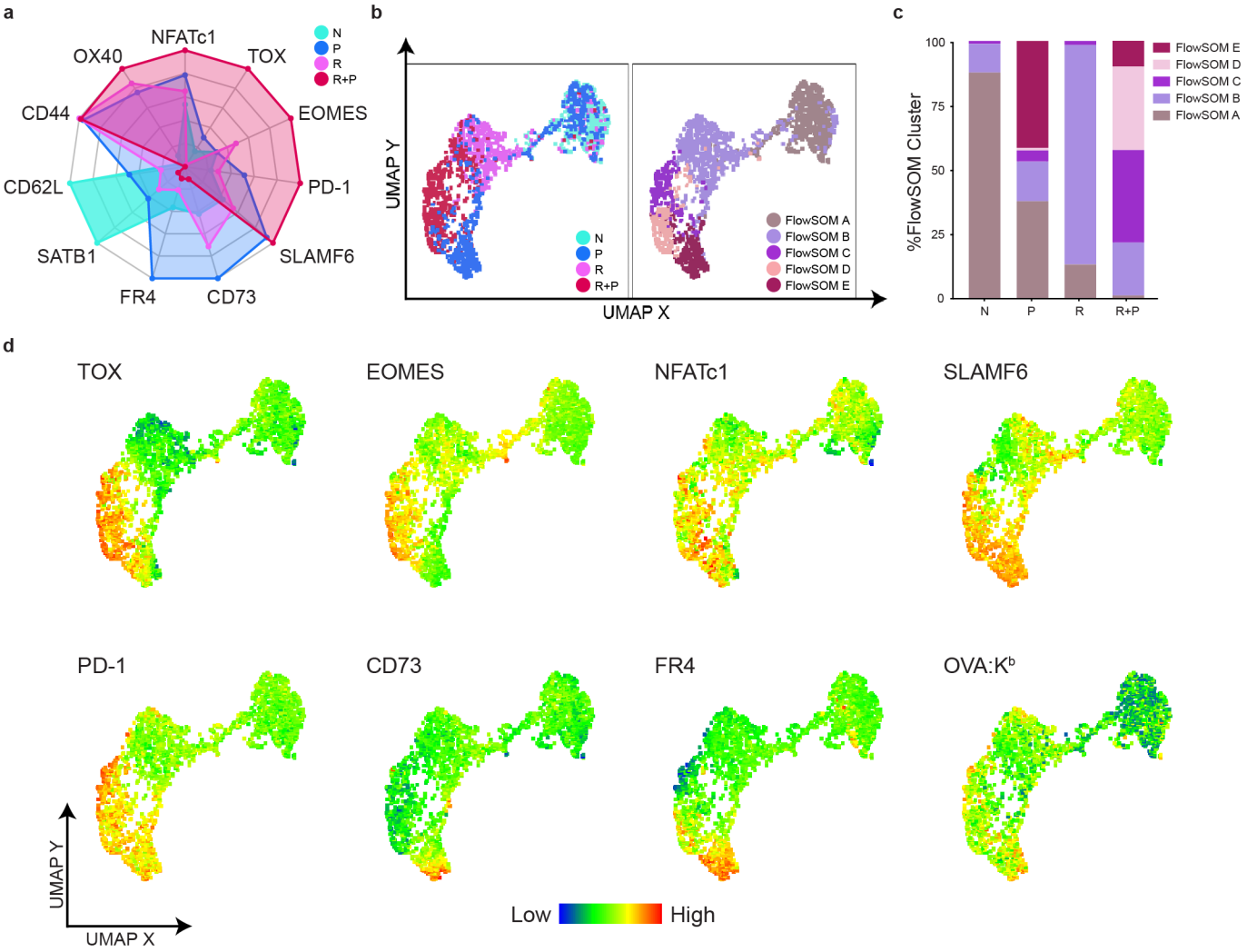
a
NFATc1
TOX
EOMES
PD-1
SLAMF6
FR4
CD73
SATB1
CD62L
CD44
OX40
N
P
R
R+P
b
UMAP Y
UMAP X
FlowSOM A
FlowSOM B
FlowSOM C
FlowSOM D
FlowSOM E
c
%FlowSOM Cluster
d
TOX
EOMES
NFATc1
SLAMF6
PD-1
CD73
FR4
OVA:Kb
Low
High

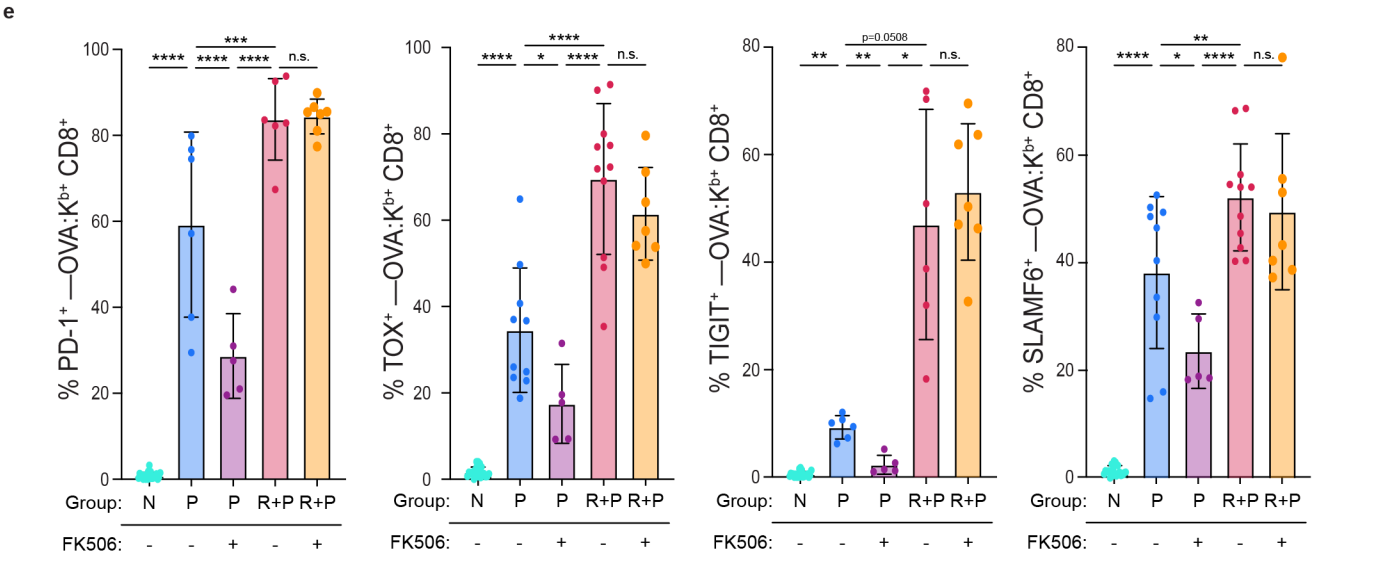
e
% PD-1+ —OVA:Kb+ CD8+
% TOX+ —OVA:Kb+ CD8+
% TIGIT+ —OVA:Kb+ CD8+
% SLAMF6+ —OVA:Kb+ CD8+
Group: N P P R+P R+P
FK506: - - + - +

Figure 5: Pregnancy programs distinct exhaustion phenotypes in memory vs. naive OVA-specific T_{FGS}. a-e, Flow cytometry panel based on RNA-seq results confirms phenotypic exhaustion in post-partum T_{FGS}. **a,** Radar plot presenting normalized expression of phenotypic markers (based on highest and lowest MFI for each marker expressed by T_{FGS} and non-T_{FGS} from all 4 experimental groups) demonstrates enhanced separation between R+P and P T_{FGS}. **b-c,** UMAP and FlowSOM reveal distinct clusters for R+P and P T_{FGS} driven by phenotypic differences in TOX, EOMES, FR4, and CD73. **d,** UMAP with heatmap overlays were generated to visualize phenotypic differences between T_{FGS} subsets. **e**, Expression levels of PD-1, TOX, TIGIT and SLAMF6 by memory vs. naive T_{FGS} from dams treated with FK506, an inhibitor of NFAT. P values were determined by one-way ANOVA; *P<0.05; **P<0.01; ****P<0.0001.

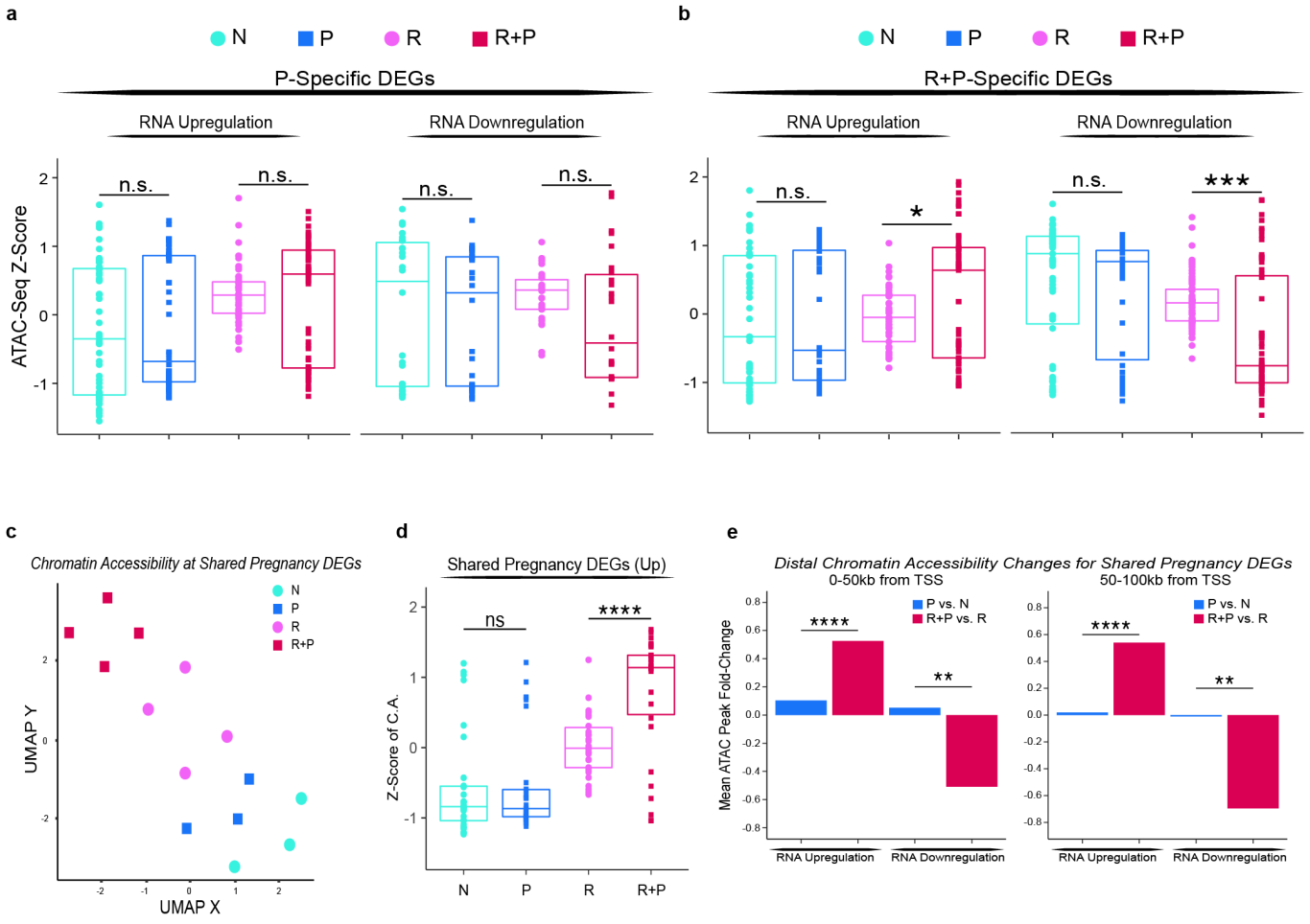
a
N
P
R
R+P
P-Specific DEGs
RNA Upregulation
RNA Downregulation
ATAC-Seq Z-Score
n.s.
b
R+P-Specific DEGs
*
***
c
Chromatin Accessibility at Shared Pregnancy DEGs
UMAP Y
UMAP X
d
Shared Pregnancy DEGs (Up)
ns
****
Z-Score of C.A.
e
Distal Chromatin Accessibility Changes for Shared Pregnancy DEGs
0-50kb from TSS
50-100kb from TSS
P vs. N
R+P vs. R
**
Mean ATAC Peak Fold-Change

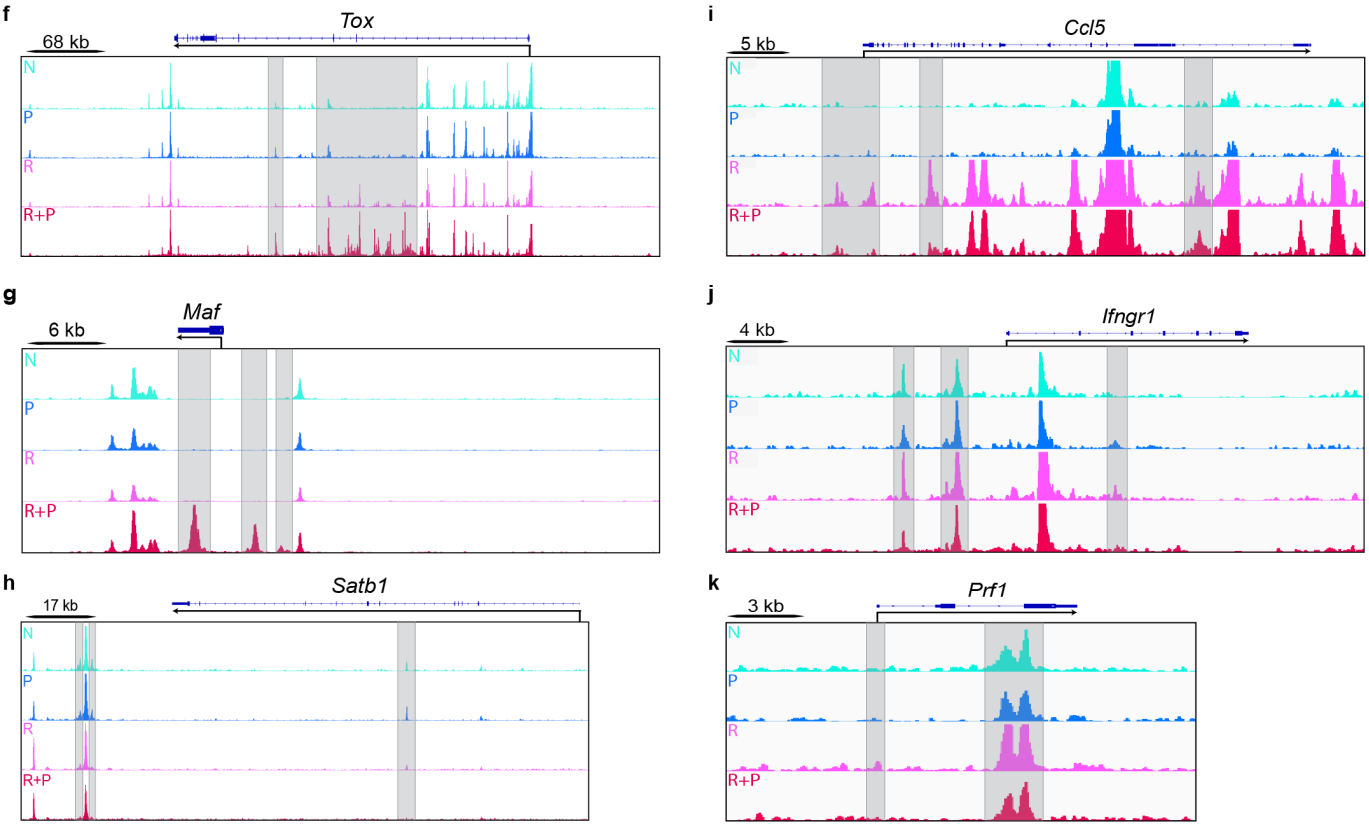
f
Tox
68 kb
i
Ccl5
5 kb
g
Maf
6 kb
j
Ifngr1
4 kb
h
Satb1
17 kb
k
Prf1
3 kb

Figure 6: Pregnancy alters the chromatin state of memory but not naive OVA-specific T_{FGS}. a-b, T_{FGS} subsets were acquired and sorted for ATAC-Seq as in **Figure 2a**. Box plots visualizing chromatin accessibility at DEGs unique to P vs. N (**a**), or unique to R+P vs. R (**b**). P values (for **a-b**) were determined by Welch's t-test. **c-d,** UMAP and box plots of chromatin accessibility at the 196 DEGs shared by P and R+P vs. R T_{FGS}. Data acquired from ≥2 biologically independent experiments with *n* = 3-4 per group. P values (for **d**) were determined by Welch's t-test. **e**, Bar plots visualizing the mean fold-change of distal ATAC-seq peaks within 0-50kb (left) or 50-100kb (right) of the TSS of shared pregnancy-induced DEGs. P vs. N T_{FGS} (blue) or R+P vs. R T_{FGS} (red). P values (for **e**) were determined by Welch's t-test. f**-h**, ATAC-Seq tracks at the *Tox*, *Maf* and *Satb1* loci, and **i-k**, *Ccl5, Ifngr1* and *Prf1*. Peaks uniquely induced in R and reversed in R+P T_{FGS} are highlighted in gray. Each dot in box plots or UMAP indicates individual mice. ns: not significant; *P<0.05; **P<0.01, ***P<0.001; ****P<0.0001.

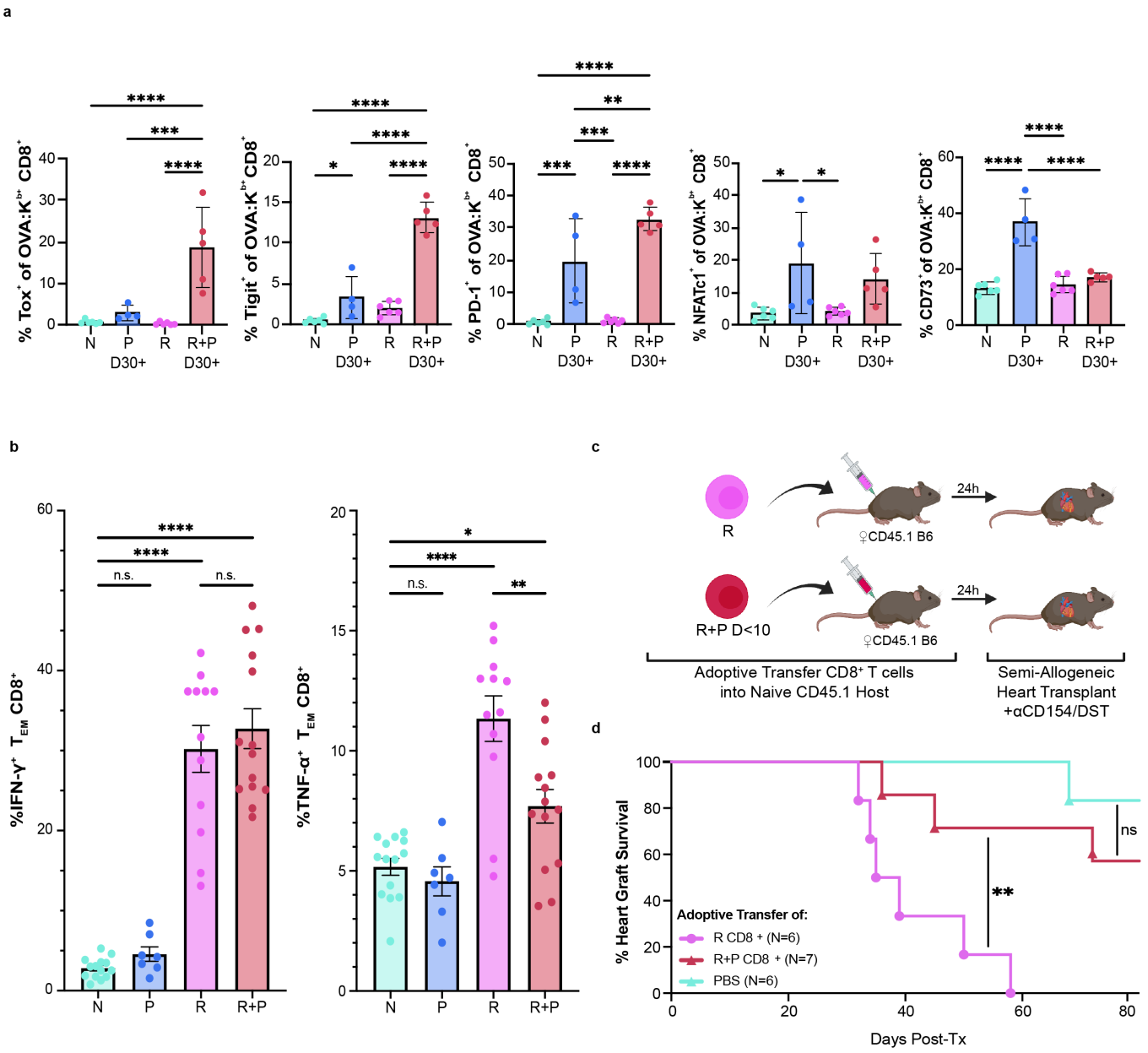

Figure 7: Pregnancy induces in memory OVA-specific T_{FGS} a sustained exhausted phenotype and restores susceptibility to co-stimulation blockade-induced acceptance of fetus-matched heart allografts. a, Percentage of OVA-specific **T_{FGS}** from P and R+P (both at post-partum day 30), Naive (N) or R (day 30-60 post-skin transplant) expressing Tox, Tigit, PD-1, NFATc1 and CD73. **b,** Bar graphs visualizing IFNγ (left) and TNFα (right) production of $CD8^+$ T_{EM} cells ($CD44^{hi}CD62L^-$) after overnight in-vitro stimulation with activated F1 APCs. Data were acquired from 2 or more biologically independent experiments; *n* = 4-13 per group. Data represent mean ± SEM. P values were determined by one-way ANOVA (for **a**), and Kruskal-Wallis test with Dunn's post hoc test (for **b**). **c**, Experimental design for adoptive transfer (AdTr) of $CD8^+$ T cells from R or R+P mice (harvested on post-partum day 0-10) into

naive CD45.1 B6 mice. 1 day after AdTr, these and PBS-control mice received allogeneic 2W-OVA.F1 (2W-OVA.B/c x B6) heart transplantation with anti-CD154/DST tolerance induction. **d**, Percentage of 2W-OVA.F1 heart graft survival among AdTr recipients; *n* = 6-7 per group. Each dot indicates individual mice. P values were determined by Mantel-Cox log-rank test. ns: not significant; *P<0.05; **P<0.01, ***P<0.001; ****P<0.0001.

REFERENCES

1. Erlebacher A. Mechanisms of T cell tolerance towards the allogeneic fetus. *Nat Rev Immunol.* 2013;13(1):23-33.
2. PrabhuDas M, Bonney E, Caron K, Dey S, Erlebacher A, Fazleabas A, et al. Immune mechanisms at the maternal-fetal interface: perspectives and challenges. *Nat Immunol.* 2015;16(4):328-34.
3. Suah AN, Tran DV, Khiew SH, Andrade MS, Pollard JM, Jain D, et al. Pregnancy-induced humoral sensitization overrides T cell tolerance to fetus-matched allografts in mice. *J Clin Invest.* 2021;131(1).
4. Kalekar LA, Schmiel SE, Nandiwada SL, Lam WY, Barsness LO, Zhang N, et al. CD4(+) T cell anergy prevents autoimmunity and generates regulatory T cell precursors. *Nature Immunology.* 2016;17(3):304-14.
5. Rowe JH, Ertelt JM, Xin L, and Way SS. Pregnancy imprints regulatory memory that sustains anergy to fetal antigen. *Nature.* 2012;490(7418):102-6.
6. Lewis EL, Xu R, Beltra JC, Ngiow SF, Cohen J, Telange R, et al. NFAT-dependent and -independent exhaustion circuits program maternal CD8 T cell hypofunction in pregnancy. *J Exp Med.* 2022;219(1).
7. Kinder JM, Turner LH, Stelzer IA, Miller-Handley H, Burg A, Shao TY, et al. CD8(+) T Cell Functional Exhaustion Overrides Pregnancy-Induced Fetal Antigen Alloimmunization. *Cell Rep.* 2020;31(12):107784.
8. Farber DL, Yudanin NA, and Restifo NP. Human memory T cells: generation, compartmentalization and homeostasis. *Nat Rev Immunol.* 2014;14(1):24-35.
9. Espinosa JR, Samy KP, and Kirk AD. Memory T cells in organ transplantation: progress and challenges. *Nat Rev Nephrol.* 2016;12(6):339-47.

10. Liu Z, Fan H, and Jiang S. CD4(+) T-cell subsets in transplantation. *Immunol Rev.* 2013;252(1):183-91.

11. Shi T, Burg AR, Caldwell JT, Roskin KM, Castro-Rojas CM, Chukwuma PC, et al. Single-cell transcriptomic analysis of renal allograft rejection reveals insights into intragraft TCR clonality. *J Clin Invest.* 2023;133(14).

12. Adams AB, Pearson TC, and Larsen CP. Heterologous immunity: an overlooked barrier to tolerance. *Immunol Rev.* 2003;196:147-60.

13. Amir AL, D'Orsogna LJ, Roelen DL, van Loenen MM, Hagedoorn RS, de Boer R, et al. Allo-HLA reactivity of virus-specific memory T cells is common. *Blood.* 2010;115(15):3146-57.

14. Benichou G. Direct and indirect antigen recognition: the pathways to allograft immune rejection. *Front Biosci.* 1999;4:D476-80.

15. Duneton C, Winterberg PD, and Ford ML. Activation and regulation of alloreactive T cell immunity in solid organ transplantation. *Nat Rev Nephrol.* 2022;18(10):663-76.

16. Valujskikh A, Pantenburg B, and Heeger PS. Primed allospecific T cells prevent the effects of costimulatory blockade on prolonged cardiac allograft survival in mice. *Am J Transplant.* 2002;2(6):501-9.

17. Yang J, Brook MO, Carvalho-Gaspar M, Zhang J, Ramon HE, Sayegh MH, et al. Allograft rejection mediated by memory T cells is resistant to regulation. *Proc Natl Acad Sci U S A.* 2007;104(50):19954-9.

18. Zhai Y, Meng L, Gao F, Busuttil RW, and Kupiec-Weglinski JW. Allograft rejection by primed/memory CD8+ T cells is CD154 blockade resistant: therapeutic implications for sensitized transplant recipients. *J Immunol.* 2002;169(8):4667-73.

19. Andrade MS, Young JS, Pollard JM, Yin D, Alegre ML, and Chong AS. Linked sensitization by memory CD4+ T cells prevents costimulation blockade-induced transplantation tolerance. *JCI Insight.* 2022;7(11).

20. Benichou G, Gonzalez B, Marino J, Ayasoufi K, and Valujskikh A. Role of Memory T Cells in Allograft Rejection and Tolerance. *Front Immunol.* 2017;8:170.

21. Gill RG, and Burrack AL. Diverse Routes of Allograft Tolerance Disruption by Memory T Cells. *Front Immunol.* 2020;11:580483.

22. Heeger PS, Greenspan NS, Kuhlenschmidt S, Dejelo C, Hricik DE, Schulak JA, et al. Pretransplant frequency of donor-specific, IFN-gamma-producing lymphocytes is a manifestation of immunologic memory and correlates with the risk of posttransplant rejection episodes. *J Immunol.* 1999;163(4):2267-75.

23. Poggio ED, Augustine JJ, Clemente M, Danzig JM, Volokh N, Zand MS, et al. Pretransplant cellular alloimmunity as assessed by a panel of reactive T cells assay correlates with acute renal graft rejection. *Transplantation.* 2007;83(7):847-52.

24. Moldenhauer LM, Diener KR, Hayball JD, and Robertson SA. An immunogenic phenotype in paternal antigen-specific CD8(+) T cells at embryo implantation elicits later fetal loss in mice. *Immunol Cell Biol.* 2017;95(8):705-15.

25. Mellor AL, Sivakumar J, Chandler P, Smith K, Molina H, Mao D, et al. Prevention of T cell-driven complement activation and inflammation by tryptophan catabolism during pregnancy. *Nat Immunol.* 2001;2(1):64-8.

26. Altman JD, and Davis MM. MHC-Peptide Tetramers to Visualize Antigen-Specific T Cells. *Curr Protoc Immunol.* 2016;115:17 3 1- 3 44.

27. Krueger LA, Nugent CT, and Hampl J. Identification of human antigen-specific T cells using MHC class I and class II tetramers. *Curr Protoc Cytom.* 2004;Chapter 6:Unit 6 18.

28. Shao TY, Kinder JM, Harper G, Pham G, Peng Y, Liu J, et al. Reproductive outcomes after pregnancy-induced displacement of preexisting microchimeric cells. *Science.* 2023;381(6664):1324-30.

29. Yu S, Zhou X, Steinke FC, Liu C, Chen SC, Zagorodna O, et al. The TCF-1 and LEF-1 transcription factors have cooperative and opposing roles in T cell development and malignancy. *Immunity.* 2012;37(5):813-26.

30. Zhou X, and Xue HH. Cutting edge: generation of memory precursors and functional memory CD8+ T cells depends on T cell factor-1 and lymphoid enhancer-binding factor-1. *J Immunol.* 2012;189(6):2722-6.

31. Giles JR, Ngiow SF, Manne S, Baxter AE, Khan O, Wang P, et al. Shared and distinct biological circuits in effector, memory and exhausted CD8(+) T cells revealed by temporal single-cell transcriptomics and epigenetics. *Nat Immunol.* 2022;23(11):1600-13.

32. Karpus WJ. Cytokines and Chemokines in the Pathogenesis of Experimental Autoimmune Encephalomyelitis. *J Immunol.* 2020;204(2):316-26.

33. Nagarsheth N, Wicha MS, and Zou W. Chemokines in the cancer microenvironment and their relevance in cancer immunotherapy. *Nat Rev Immunol.* 2017;17(9):559-72.

34. Griffith JW, Sokol CL, and Luster AD. Chemokines and chemokine receptors: positioning cells for host defense and immunity. *Annu Rev Immunol.* 2014;32:659-702.

35. Foeng J, Comerford I, and McColl SR. Harnessing the chemokine system to home CAR-T cells into solid tumors. *Cell Rep Med.* 2022;3(3):100543.

36. Blank CU, Haining WN, Held W, Hogan PG, Kallies A, Lugli E, et al. Defining 'T cell exhaustion'. *Nat Rev Immunol.* 2019;19(11):665-74.

37. Khan O, Giles JR, McDonald S, Manne S, Ngiow SF, Patel KP, et al. TOX transcriptionally and epigenetically programs CD8(+) T cell exhaustion. *Nature.* 2019;571(7764):211-8.

38. Bengsch B, Ohtani T, Herati RS, Bovenschen N, Chang KM, and Wherry EJ. Deep immune profiling by mass cytometry links human T and NK cell differentiation and cytotoxic molecule expression patterns. *J Immunol Methods.* 2018;453:3-10.

39. Schietinger A, Philip M, Krisnawan VE, Chiu EY, Delrow JJ, Basom RS, et al. Tumor-Specific T Cell Dysfunction Is a Dynamic Antigen-Driven Differentiation Program Initiated Early during Tumorigenesis. *Immunity.* 2016;45(2):389-401.

40. Scott AC, Dundar F, Zumbo P, Chandran SS, Klebanoff CA, Shakiba M, et al. TOX is a critical regulator of tumour-specific T cell differentiation. *Nature.* 2019;571(7764):270-4.

41. Philip M, Fairchild L, Sun L, Horste EL, Camara S, Shakiba M, et al. Chromatin states define tumour-specific T cell dysfunction and reprogramming. *Nature.* 2017;545(7655):452-6.

42. Russ BE, Olshanksy M, Smallwood HS, Li J, Denton AE, Prier JE, et al. Distinct epigenetic signatures delineate transcriptional programs during virus-specific CD8(+) T cell differentiation. *Immunity.* 2014;41(5):853-65.

43. Zhang JA, Mortazavi A, Williams BA, Wold BJ, and Rothenberg EV. Dynamic transformations of genome-wide epigenetic marking and transcriptional control establish T cell identity. *Cell.* 2012;149(2):467-82.

44. Montacchiesi G, and Pace L. Epigenetics and CD8(+) T cell memory. *Immunol Rev.* 2022;305(1):77-89.

45. Abdel-Hakeem MS, Manne S, Beltra JC, Stelekati E, Chen Z, Nzingha K, et al. Epigenetic scarring of exhausted T cells hinders memory differentiation upon eliminating chronic antigenic stimulation. *Nat Immunol.* 2021;22(8):1008-19.

46. Braun M, Ress ML, Yoo YE, Scholz CJ, Eyrich M, Schlegel PG, et al. IL12-mediated sensitizing of T-cell receptor-dependent and -independent tumor cell killing. *Oncoimmunology.* 2016;5(7):e1188245.

47. Belarif L, Mary C, Jacquemont L, Mai HL, Danger R, Hervouet J, et al. IL-7 receptor blockade blunts antigen-specific memory T cell responses and chronic inflammation in primates. *Nat Commun.* 2018;9(1):4483.

48. Belk JA, Yao W, Ly N, Freitas KA, Chen YT, Shi Q, et al. Genome-wide CRISPR screens of T cell exhaustion identify chromatin remodeling factors that limit T cell persistence. *Cancer Cell.* 2022;40(7):768-86 e7.

49. Pearce EL, and Shen H. Generation of CD8 T cell memory is regulated by IL-12. *J Immunol.* 2007;179(4):2074-81.

50. Giordano M, Henin C, Maurizio J, Imbratta C, Bourdely P, Buferne M, et al. Molecular profiling of CD8 T cells in autochthonous melanoma identifies Maf as driver of exhaustion. *EMBO J.* 2015;34(15):2042-58.

51. Yao C, Sun HW, Lacey NE, Ji Y, Moseman EA, Shih HY, et al. Single-cell RNA-seq reveals TOX as a key regulator of CD8(+) T cell persistence in chronic infection. *Nat Immunol.* 2019;20(7):890-901.

52. Stephen TL, Payne KK, Chaurio RA, Allegrezza MJ, Zhu H, Perez-Sanz J, et al. SATB1 Expression Governs Epigenetic Repression of PD-1 in Tumor-Reactive T Cells. *Immunity.* 2017;46(1):51-64.

53. Best JA, Blair DA, Knell J, Yang E, Mayya V, Doedens A, et al. Transcriptional insights into the CD8(+) T cell response to infection and memory T cell formation. *Nat Immunol.* 2013;14(4):404-12.

54. Yates KB, Tonnerre P, Martin GE, Gerdemann U, Al Abosy R, Comstock DE, et al. Epigenetic scars of CD8(+) T cell exhaustion persist after cure of chronic infection in humans. *Nat Immunol.* 2021;22(8):1020-9.

55. Chen Y, Zander R, Khatun A, Schauder DM, and Cui W. Transcriptional and Epigenetic Regulation of Effector and Memory CD8 T Cell Differentiation. *Front Immunol.* 2018;9:2826.

56. Miller ML, McIntosh CM, Williams JB, Wang Y, Hollinger MK, Isaad NJ, et al. Distinct Graft-Specific TCR Avidity Profiles during Acute Rejection and Tolerance. *Cell Rep.* 2018;24(8):2112-26.

57. Bediaga NG, Coughlan HD, Johanson TM, Garnham AL, Naselli G, Schroder J, et al. Multi-level remodelling of chromatin underlying activation of human T cells. *Sci Rep.* 2021;11(1):528.

58. Wang W, Sung N, Gilman-Sachs A, and Kwak-Kim J. T Helper (Th) Cell Profiles in Pregnancy and Recurrent Pregnancy Losses: Th1/Th2/Th9/Th17/Th22/Tfh Cells. *Front Immunol.* 2020;11:2025.

59. Sojka DK, Yang L, and Yokoyama WM. Uterine Natural Killer Cells. *Front Immunol.* 2019;10:960.

60. Ashkar AA, Di Santo JP, and Croy BA. Interferon gamma contributes to initiation of uterine vascular modification, decidual integrity, and uterine natural killer cell maturation during normal murine pregnancy. *J Exp Med.* 2000;192(2):259-70.

61. Torchinsky A, Shepshelovich J, Orenstein H, Zaslavsky Z, Savion S, Carp H, et al. TNF-alpha protects embryos exposed to developmental toxicants. *Am J Reprod Immunol.* 2003;49(3):159-68.

62. Guillonneau C, Hill M, Hubert FX, Chiffoleau E, Herve C, Li XL, et al. CD40Ig treatment results in allograft acceptance mediated by CD8CD45RC T cells, IFN-gamma, and indoleamine 2,3-dioxygenase. *J Clin Invest.* 2007;117(4):1096-106.

63. Markees TG, Phillips NE, Gordon EJ, Noelle RJ, Shultz LD, Mordes JP, et al. Long-term survival of skin allografts induced by donor splenocytes and anti-CD154 antibody in thymectomized mice requires CD4(+) T cells, interferon-gamma, and CTLA4. *J Clin Invest.* 1998;101(11):2446-55.

64. Rudloff MW, Zumbo P, Favret NR, Roetman JJ, Detres Roman CR, Erwin MM, et al. Hallmarks of CD8(+) T cell dysfunction are established within hours of tumor antigen encounter before cell division. *Nat Immunol.* 2023;24(9):1527-39.

65. Burns AM, Ma L, Li Y, Yin D, Shen J, Xu J, et al. Memory alloreactive B cells and alloantibodies prevent anti-CD154-mediated allograft acceptance. *J Immunol.* 2009;182(3):1314-24.

66. Picelli S, Faridani OR, Bjorklund AK, Winberg G, Sagasser S, and Sandberg R. Full-length RNA-seq from single cells using Smart-seq2. *Nat Protoc.* 2014;9(1):171-81.

67. Martin M. Cutadapt removes adapter sequeces from high-throughput sequencing reads. *EMBnetjournal.* 2011;1791):10.

68. Dobin A, Davis CA, Schlesinger F, Drenkow J, Zaleski C, Jha S, et al. STAR: ultrafast universal RNA-seq aligner. *Bioinformatics.* 2013;29(1):15-21.

69. Liao Y, Smyth GK, and Shi W. featureCounts: an efficient general purpose program for assigning sequence reads to genomic features. *Bioinformatics.* 2014;30(7):923-30.

70. Buenrostro JD, Giresi PG, Zaba LC, Chang HY, and Greenleaf WJ. Transposition of native chromatin for fast and sensitive epigenomic profiling of open chromatin, DNA-binding proteins and nucleosome position. *Nat Methods.* 2013;10(12):1213-8.

71. Mandal M, Hamel KM, Maienschein-Cline M, Tanaka A, Teng G, Tuteja JH, et al. Histone reader BRWD1 targets and restricts recombination to the Igk locus. *Nat Immunol.* 2015;16(10):1094-103.

72. Langmead B, and Salzberg SL. Fast gapped-read alignment with Bowtie 2. *Nat Methods.* 2012;9(4):357-9.

73. Barnett DW, Garrison EK, Quinlan AR, Stromberg MP, and Marth GT. BamTools: a C++ API and toolkit for analyzing and managing BAM files. *Bioinformatics.* 2011;27(12):1691-2.

74. . Picard Toolkit (Broad Institute, https://broadinstitute.github.io/picard/, 2019).

75. Newell R, Pienaar R, Balderson B, Piper M, Essebier A, and Boden M. ChIP-R: Assembling reproducible sets of ChIP-seq and ATAC-seq peaks from multiple replicates. *Genomics.* 2021;113(4):1855-66.

76. Quinlan AR, and Hall IM. BEDTools: a flexible suite of utilities for comparing genomic features. *Bioinformatics.* 2010;26(6):841-2.

77. Ramirez F, Dundar F, Diehl S, Gruning BA, and Manke T. deepTools: a flexible platform for exploring deep-sequencing data. *Nucleic Acids Res.* 2014;42(Web Server issue):W187-91.

78. Lawrence M, Huber W, Pages H, Aboyoun P, Carlson M, Gentleman R, et al. Software for computing and annotating genomic ranges. *PLoS Comput Biol.* 2013;9(8):e1003118.

79. Zhu LJ, Gazin C, Lawson ND, Pages H, Lin SM, Lapointe DS, et al. ChIPpeakAnno: a Bioconductor package to annotate ChIP-seq and ChIP-chip data. *BMC Bioinformatics.* 2010;11:237.

80. Love MI, Huber W, and Anders S. Moderated estimation of fold change and dispersion for RNA-seq data with DESeq2. *Genome Biol.* 2014;15(12):550.

81. Heinz S, Benner C, Spann N, Bertolino E, Lin YC, Laslo P, et al. Simple combinations of lineage-determining transcription factors prime cis-regulatory elements required for macrophage and B cell identities. *Mol Cell.* 2010;38(4):576-89.

82. Robinson JT, Thorvaldsdottir H, Winckler W, Guttman M, Lander ES, Getz G, et al. Integrative genomics viewer. *Nat Biotechnol.* 2011;29(1):24-6.

83. Zhou Y, Zhou B, Pache L, Chang M, Khodabakhshi AH, Tanaseichuk O, et al. Metascape provides a biologist-oriented resource for the analysis of systems-level datasets. *Nat Commun.* 2019;10(1):1523.